568340

Chapter TBD

ABSENCE OF MINERAL COLLOIDS IN HIGH IONIC STRENGTH SOLUTIONS ASSOCIATED WITH SALT FORMATIONS: EXPERIMENTAL DETERMINATION AND APPLICATIONS TO NUCLEAR WASTE MANAGEMENT. Final

MDL 06/30/2017

Yongliang Xiong [1*], Leslie Kirkes [1], Sungtae Kim [1], Cassie Marrs [1], Jandi Knox [1], Justin Dean [1], Haoran Deng [2], Martin Nemer [2 *]

[1] Sandia National Laboratories (SNL), Carlsbad Programs Group, 4100 National Parks Highway, Carlsbad, NM 88220, USA

[2] Sandia National Laboratories (SNL), Albuquerque, P.O. Box 5800, NM 87185, USA

ABSTRACT

Radionuclides and heavy metals easily sorb onto colloids. This phenomenon can have a beneficial impact on environmental clean-up activities if one is trying to scavenge hazardous elements from soil for example. On the other hand, it can have a detrimental impact in cases where one is trying to immobilize these hazardous elements and keep them isolated from the public. Such is the case in the field of radioactive waste disposal. Colloids in the aqueous phase in a radioactive waste repository could facilitate transport of contaminants including radioactive nuclides.

* Corresponding Author address
Email: yxiong@sandia.gov

SAND2017-6865B

WIPP: 4.4.2.21 :PUB:QA-L:SAND2017-6865B

Salt formations have been recommended for nuclear waste isolation since the 1950's by the U.S. National Academy of Science. In this capacity, salt formations are ideal for isolation of radioactive waste. However, salt formations contain brine (the aqueous phase), and colloids could possibly be present. If present in the brines associated with salt formations, colloids are highly relevant to the isolation safety concept for radioactive waste.

The Waste Isolation Pilot Plant (WIPP) in southeast New Mexico is a premier example where a salt formation is being used as the primary isolation barrier for radioactive waste. WIPP is a U.S. Department of Energy geological repository for the permanent disposal of defense-related transuranic (TRU) waste. In addition to the geological barrier that the bedded salt formation provides, an engineered barrier of MgO added to the disposal rooms is used in WIPP. Industrial-grade MgO, consisting mainly of the mineral periclase, is in fact the only engineered barrier certified by the U.S. Environmental Protection Agency (EPA) for emplacement in the WIPP.

Of interest, an $Mg(OH)_2$-based engineered barrier consisting mainly of the mineral brucite is to be employed in the Asse repository in Germany. The Asse repository is located in a domal salt formation and is another example of using salt formations for disposal of radioactive waste.

Should colloids be present in salt formations, they would facilitate transport of contaminants including actinides. In the case of colloids derived from emplaced MgO, it is the hydration and carbonation products that are of interest. These colloids could possibly form under conditions relevant in particular to the WIPP.

In this chapter, we report a systematic experimental study performed at Sandia National Laboratories in Carlsbad, New Mexico, related to the WIPP engineered barrier, MgO. The aim of this work is to confirm the presence or absence of mineral fragment colloids related to MgO in high ionic strength solutions (brines). The results from such a study provides information about the stability of colloids in high ionic strength solutions in general, not just for the WIPP.

We evaluated the possible formation of mineral fragment colloids using two approaches. The first approach is an analysis of long-term MgO hydration and carbonation experiments performed at Sandia National Laboratories (SNL) as a function of equivalent pore sizes. The MgO hydration products include $Mg(OH)_2$ (brucite) and $Mg_3Cl(OH)_5 \cdot 4H_2O$ (phase 5), and the carbonation product includes $Mg_5(CO_3)_4(OH)_2 \cdot 4H_2O$ (hydromagnesite). All these phases contain magnesium. Therefore, if mineral fragment colloids of these hydration and carbonation products were formed in the SNL experiments

mentioned above, magnesium concentrations in the filtrate from the experiments would show a dependence on ultrafiltration. In other words, there would be a decrease in magnesium concentrations as a function of ultrafiltration with decreasing molecular weight (MW) cut-offs for the filtration. Therefore, we performed ultrafiltration on solution samples from the SNL hydration and carbonation experiments as a function of equivalent pore size.

We filtered solutions using a series of MW cut-off filters at 100 kD, 50 kD, 30 kD and 10 kD. Our results demonstrate that the magnesium concentrations remain constant with decreasing MW cut-offs, implying the absence of mineral fragment colloids.

The second approach uses spiked Cs^+ to indicate the possible presence of mineral fragment colloids. Cs^+ is easily absorbed by colloids. Therefore, we added Cs^+ to a subset of SNL MgO hydration and carbonation experiments. Again, we filtered the solutions with a series of MW cut-off filters at 100 kD, 50 kD, 30 kD and 10 kD. This time we measured the concentrations of Cs. The concentrations of Cs do not change as a function of MW cut-offs, indicating the absence of colloids from MgO hydration and carbonation products. Therefore, both approaches demonstrate the absence of mineral fragment colloids from MgO hydration and carbonation products.

Based on our experimental results, we acknowledge that mineral fragment colloids were not formed in the SNL MgO hydration and carbonation experiments, and we further conclude that high ionic strength solutions associated with salt formations prevent the formation of mineral fragment colloids. This is due to the fact that the high ionic strength solutions associated with salt formations have high concentrations of both monovalent and divalent metal ions that are orders of magnitude higher than the critical coagulation concentrations for mineral fragment colloids. The absence of mineral fragment colloids in high ionic strength solutions implies that contributions from mineral fragment colloids to the total mobile source term of radionuclides in a salt repository are minimal.

Keywords: Nuclear Waste Management; Colloidal Transport; Environmental Chemistry; Engineered Barrier; Waste Isolation Pilot Plant (WIPP);

INTRODUCTION

A colloid is a dispersed, separable phase that is suspended within a second phase, in this case, aqueous brine solutions. In this study, we follow the operational terminology defined by Ross and Sherrell (1999) regarding colloidal

and dissolved fractions; i.e., the colloidal fraction can be separated from solution using filters/ultrafilters with pore sizes ranging from 10 kDa to 0.2 μm.

Colloids can facilitate transport of contaminants including actinides (e.g., Wen et al., 1999), and therefore, the possible persistence of colloids is important in performance of the isolation characteristic of a nuclear waste repository. The persistence of colloids may increase actinide mobility and enhance transport of actinides.

Salt formations are ideal for nuclear waste isolation, as recommended by the National Academy of Science as early as the 1950's (U.S. National Academy of Science, 1957), as salt formations have the following advantages: (1) low permeability; (2) plastic deformation after closure of a repository to encapsulate wastes, (3) self-healing of fractures, and (4) high thermal conductivity of salt.

There are four types of colloids considered in the conceptual model for the Waste Isolation Pilot Plant (WIPP), a nuclear waste repository in a bedded salt formation, located in southeast New Mexico. These are: intrinsic colloids, mineral fragment colloids, humic colloids, and biocolloids. Intrinsic colloids are generated by polymerization of actinides via hydrolysis. When actinide elements (intrinsic colloids or aqueous species) are absorbed onto inorganic or organic aquatic colloids because of their affinity to these colloids, the final products become actinide pseudocolloids (e.g., Olofsson and Allard, 1986). Mineral fragment colloids are pseudocolloids formed by sorption of aqueous actinide species or intrinsic actinide colloids onto inorganic aquatic colloids (Zhao and Steward, 1997). Aquatic colloids that can absorb aqueous actinide species or intrinsic actinide colloids may be inorganic or organic. Humic substance is an example of aquatic organic colloids (Kim et al., 1994). Various mineral fragments, such as α-Al_2O_3 (Olofsson et al., 1983), bentonite (Kelly et al., 1996), hematite and goethite (Itagaki et al., 1991; Kelly et al., 1996), montmorillonite (Olofsson and Allard, 1986); SiO_2 (Allen and Matijević, 1969, 1971; Olofsson and Allard, 1986; Itagaki et al., 1991), and ZrO_2 (Bitea et al., 2003), are examples of aquatic inorganic colloids.

The stability of both intrinsic colloids and pseudocolloids, highly depends on the ionic strength of the aqueous solution (Allen and Matijević, 1969, 1971; van Olphen, 1991). The ionic strength at which rapid destabilization and agglomeration of both intrinsic colloids and pseudocolloids occurs is referred to as the critical coagulation concentration, c.c.c. Regarding the c.c.c. required for mineral fragment colloids, electrolytes containing monovalent cations such as Na^+ and K^+ have a higher c.c.c. up to 0.15 M (van Olphen, 1991). In contrast, electrolytes containing divalent cations such as Mg^{2+} and Ca^{2+} have a much lower c.c.c., ranging from 5×10^{-4} to 2×10^{-3} M (van Olphen, 1991).

Solutions associated with salt formations are characterized by high ionic strengths. For example, in the WIPP, there are two brines considered for the performance of the repository, i.e., Generic Weep Brine (GWB), and Energy Research and Development Administration (WIPP Well) 6 (ERDA-6). They have ionic strengths of 8.26 $mol \cdot kg^{-1}$ and 5.82 $mol \cdot kg^{-1}$, respectively (Xiong and Lord, 2008). In the Asse, the brine used for assessing performance is the Q-brine, an Mg-Cl dominated brine with an ionic strength of ~13 $mol \cdot kg^{-1}$ (Schuessler et al., 2000). In such high ionic strength solutions with multiple components, it is expected that the formation of mineral fragment colloids is unlikely, but has not been experimentally demonstrated.

In work performed by Altmaier et al. (2004), the authors suggested the potential formation of mineral fragment colloids composed of magnesium chloride hydroxide hydrate in pure $MgCl_2$ solutions. There are two types of magnesium chloride hydroxide hydrates that are typically observed, i.e., $Mg_2Cl(OH)_3 \cdot 4H_2O$ (called phase 3 in the cement industry) and $Mg_3Cl(OH)_5 \cdot 4H_2O$ (called phase 5 in the cement industry). Altmaier et al. (2004) concluded that Th(IV) could adsorb to phase 3 mineral fragments to form actinide pseudocolloids.

In the WIPP near field geochemical model there are two types of brines, ERDA-6 and GWB. GWB is a Na-Mg-Cl dominated brine, and ERDA-6 is a Na-Cl dominated brine. These brines are characterized by high ionic strengths, with GWB and ERDA-6 having ionic strengths of 8.26 $mol \cdot kg^{-1}$ and 5.82 $mol \cdot kg^{-1}$, respectively (Xiong and Lord, 2008). These brines are multi-component, and are significantly different from pure $MgCl_2$ solutions used in the experiments of Altmaier et al. (2004). These brines have high concentrations of both monovalent and divalent ions. For example, the ERDA-6 brine has 5.35 $mol \cdot kg^{-1}$, 0.106 $mol \cdot kg^{-1}$, 0.0209 $mol \cdot kg^{-1}$, 0.0132 $mol \cdot kg^{-1}$ for Na^+, K^+, Mg^{2+}, and Ca^{2+} (Xiong and Lord, 2008), respectively. Similarly, GWB has 4.04 $mol \cdot kg^{-1}$, 0.532 $mol \cdot kg^{-1}$, 1.16 $mol \cdot kg^{-1}$, 0.0163 $mol \cdot kg^{-1}$ for Na^+, K^+, Mg^{2+}, and Ca^{2+} (Xiong and Lord, 2008), respectively. These concentrations are much higher than the c.c.c. mentioned above, implying that any mineral fragments and their pseudocolloids are unstable in these brines. The presence of both monovalent and divalent cations in the WIPP brines is important. In fact, Altmaier et al. (2004) mentioned that "in NaCl or dilute $MgCl_2$ solutions, neither solid $Mg_2(OH)_3Cl \cdot 4H_2O(s)$ nor its colloids are stable." Therefore, the chemical compositions of the brine solutions make it unlikely that magnesium chloride hydroxide hydrate colloids would form (Xiong, Brush, Garner, and Long, 2010), but to this date the stability of these colloids has not been demonstrated.

When industrial grade MgO is added as an engineered barrier to react with GWB, only phase 5 is formed (Xiong and Lord, 2008). However, when the ERDA-6 brine reacts with industrial grade MgO, neither phase 5 nor phase 3 is observed (Xiong and Lord, 2008). These observations are in agreement with thermodynamic calculations (Xiong et al., 2010b). Therefore, it has been reasoned that colloidal suspensions of either phase 3 or phase 5 are not a concern in the ERDA-6 brine. In the presence of CO_2(g), when GWB and ERDA-6 react with MgO, hydromagnesite forms (Xiong and Lord, 2008).

The objective of this work is to experimentally evaluate the possible presence of mineral fragment colloids in high ionic strength solutions associated with salt formations, with a special reference to the possible presence of mineral fragment colloids resulting from the reaction of MgO with WIPP brines, including hydration and carbonation products. The results from this study will also have broad applications to other geological repositories in salt formations in general.

METHODS

Experimental Design

In this work, we investigated the possible presence of mineral fragment colloids by using the method of ultrafiltration. We designed two sets of experiments for this purpose. In the first set of experiments, we withdraw five aliquots of solution samples from long-term MgO hydration or carbonation experiments, which were set-up in 2008 in various solutions including synthetic GWB and ERDA-6 (see Tables 1 and 2 for details) at Sandia National Laboratories (SNL) in Carlsbad, NM (Deng, Nemer, Xiong, 2006; Deng, Xiong, Nemer, Johnsen, 2009). Then, each aliquot is separately subject to phase separation with filtration and ultrafiltration corresponding to 0.2 μm and molecular weight (MW) cut-off filters at 100 kD, 50 kD, 30 kD and 10 kD. Then, these samples were analyzed for Mg using inductively coupled plasma atomic emission spectrometer (ICP-AES). Theoretically, if colloids are present, we would expect to see a significant drop in Mg concentrations after filtration and a consistently lower concentration of Mg in successive filtrations as Mg-bearing colloids are retained by filtration, as the hydration products, $Mg(OH)_2$ (brucite), and $Mg_3Cl(OH)_5 \cdot 4H_2O$ (phase 5), and the carbonation product, $Mg_5(CO_3)_4(OH)_2 \cdot 4H_2O$ (hydromagnesite), contain magnesium.

In the second set of experiments, we introduced the tracer, a CsCl solution, into solution samples taken from the same long-term experiments (Deng, Nemer, Xiong, 2006; Deng, Xiong, Nemer, Johnsen, 2009), to detect the

presence of colloids. It has been repeatedly demonstrated that Cs^+ is easily absorbed onto various colloids (e.g., Bascetin et al., 2003; Chen et al., 2005). Again, we withdraw five aliquots of solution samples with CsCl added. Then, each aliquot is separately subject to phase separation with filtration and ultrafiltration corresponding to 0.2 μm and MW cut-off filters at 100 kD, 50 kD, 30 kD and 10 kD. After that, solution samples were analyzed for Cs using inductively coupled plasma mass spectrometer (ICP-MS). Theoretically, if mineral fragment colloids are present, we would expect to see a significant drop in Cs concentrations as a function of decreasing equivalent pore sizes, because mineral fragment colloids with Cs^+ absorbed onto them are retained by filtration and ultrafiltration.

If we observe a decrease in Mg and Cs concentrations as a function of decreasing equivalent pore sizes in these experiments, it indicates the presence of mineral fragment colloids. Conversely, if there is no dependence in Mg and Cs concentrations on decreasing equivalent pore sizes, i.e., Mg and Cs concentrations remain constant regardless of equivalent pore sizes, it indicates the absence of any mineral fragment colloids.

Analytical Equipment and Experimental Material

Ultrafiltration devices, Amicon® Ultra centrifugal filters, for this work are from *MilliporeSigma* Company. The ultrafiltration devices used in experiments include MW cut-off ultrafilters at 100 kD, 50 kD, 30 kD and 10 kD, corresponding to equivalent pore sizes of 7, 5, 4, and 3 nanometers (nm), respectively. The centrifuge used in experiments for ultrafiltration was an Avanti® J-E centrifuge from Beckman Coulter Company.

Elemental concentrations of magnesium were determined by using the Perkin Elmer Optima DV 3300 inductively coupled plasma atomic emission spectrometer (ICP-AES). The Perkin Elmer NexIon 300D inductively coupled plasma mass spectrometer (ICP-MS) is being used for determination of elemental concentrations of cesium.

The industrial grade MgO used in long-term hydration and carbonation experiments were from Martin Marietta Magnesia Specialties LLC (Deng et al., 2008, 2009). The distributions of particle sizes for the industrial grade MgO were as follows: > 2 mm, 7.02±0.91 wt%; 1 mm—2 mm, 32.52±1.78 wt%; 600 μm—1 mm, 20.25±1.28 wt%; 300 μm—600 μm, 12.74±2.19 wt%; 150 μm—300 μm, 5.35±0.70 wt%; 75 μm—150 μm, 3.36±0.35 wt%; and < 75 μm, 17.91±1.88 wt% (Deng et al., 2008). The chemical compositions of the industrial grade MgO were 98.46±2.54 wt% of MgO; 0.87±0.03 wt% of CaO; 0.13±0.018 wt% of Al_2O_3;

0.12±0.01 wt% of total iron oxide; and 0.31±0.01 wt% of SiO_2 (Deng et al., 2008). The MgO with three particle sizes were used in experiments: (1) as-received MgO (mixed size MgO); (2) large particle size MgO (1 mm—2 mm); and small particle size MgO (< 75 μm).

The GWB and ERDA-6 used in long-term hydration and carbonation experiments were synthesized according to the recipes (Xiong, 2008). The chemicals used for making the synthetic GWB and ERDA-6 were reagent grade chemicals from Fisher Scientific. In addition, 1.0 M $MgCl_2$ solution was used in long-term hydration experiments, and simplified GWB (1.0 M $MgCl_2$ + 3.6 M NaCl) was used for both long-term hydration and carbonation experiments.

EXPERIMENTAL RESULTS

Magnesium Concentrations as a Function of Equivalent Pore Sizes

In this section, magnesium concentrations as a function of equivalent pore size for samples taken from the SNL MgO long-term hydration and carbonation experiments in GWB and ERDA-6 are presented. It should be mentioned that the hydration products for MgO hydration experiments in GWB are phase 5 and brucite, whereas the hydration product in ERDA-6 is brucite (Xiong and Lord, 2008). The carbonation product for MgO carbonation experiments in both GWB and EDRA-6 is hydromagnesite(5424) (Xiong and Lord, 2008). In MgO carbonation experiments, hydration products characteristic of GWB and ERDA-6, as mentioned before, are also present.

In addition, the hydration products for MgO long-term hydration experiments with a 1.0 M $MgCl_2$ solution are brucite and phase 5. The hydration and carbonation products for the experiments with the simplified GWB are identical to those with GWB.

In Figures 1 and 2, magnesium concentrations as a function of ultrafiltration in terms of equivalent pore size in nano meter for long-term MgO hydration experiments in GWB for large particle size MgO are shown. The equivalent pore sizes used in experiments for phase separation range from 3 nm to 200 nm. Figures 1 and 2 indicate that magnesium concentrations remain constant over this range of equivalent pore sizes, suggesting the absence of mineral fragment colloids from MgO hydration products in experiments with large particle size MgO.

Magnesium concentrations as a function of ultrafiltration for long-term MgO hydration experiments in 1.0 M $MgCl_2$ are presented in Figures 3 and 4. These experiments covered three particle sizes of MgO—mixed (i.e., as-received) particle size MgO, large particle size MgO and small particle size MgO. Figures 3 and 4 demonstrate that magnesium concentrations remain constant regardless of ultrafiltration, suggesting the absence of mineral fragment colloids from MgO hydration products in 1.0 M $MgCl_2$.

In Figures 5 and 6, magnesium concentrations as a function of ultrafiltration for long-term MgO carbonation experiments in GWB are displayed. These experiments were conducted at $P_{CO_2} = 3.5 \times 10^{-4}$ atm with mixed (i.e., as-received) particle size MgO. Figures 5 and 6 indicate that magnesium concentrations remain constant regardless of ultrafiltration, suggesting the absence of mineral fragment colloids from both MgO hydration and carbonation products in GWB.

In Figures 7 through 9, magnesium concentrations as a function of ultrafiltration for long-term MgO carbonation experiments in GWB are depicted. These experiments were conducted at $P_{CO_2} = 3.5 \times 10^{-3}$ atm with mixed particle size MgO. These figures indicate that magnesium concentrations remain constant regardless of ultrafiltration, suggesting the absence of mineral fragment colloids from both MgO hydration and carbonation products in GWB.

In Figures 10 through 12, the results from the carbonation experiments conducted at $P_{CO_2} = 3.5 \times 10^{-3}$ atm with large particle size MgO in GWB are shown. These figures indicate that magnesium concentrations remain constant regardless of ultrafiltration.

Figures 13 and 14 are similar to Figures 10 through 12, except that the results refer to the carbonation experiments conducted at $P_{CO_2} = 3.5 \times 10^{-3}$ atm with mixed particle size MgO in simplified GWB.

In Figure 15, the results from the carbonation experiments conducted at $P_{CO_2} = 3.5 \times 10^{-4}$ atm with prehydrated mixed particle size MgO in GWB are presented. In these experiments, MgO was prehydrated as brucite and phase 5. Therefore, these experiments actually investigated the direct carbonation of MgO from its hydration products. These experimental results indicate that magnesium concentrations remain constant regardless of ultrafiltration, suggesting the absence of mineral fragment colloids from both MgO hydration and carbonation products in GWB.

The experimental results presented in Figure 16 are similar to those in Figure 15, except that the results in Figure 16 are from the carbonation experiments

conducted at $P_{CO_2} = 3.5 \times 10^{-4}$ atm with prehydrated mixed particle size MgO in simplified GWB.

In Figures 17 and 18, magnesium concentrations as a function of ultrafiltration for long-term MgO carbonation experiments in ERDA-6 are displayed. These experiments were conducted at $P_{CO_2} = 3.5 \times 10^{-3}$ atm with small particle size MgO. Figures 17 and 18 indicate that magnesium concentrations remain constant regardless of ultrafiltration, suggesting the absence of mineral fragment colloids from both MgO hydration and carbonation products in EDRA-6.

Cesium Concentrations as a Function of Equivalent Pore Sizes

In the following, cesium concentrations as a function of equivalent pore size for samples taken from the SNL long-term MgO hydration and carbonation experiments in various solutions are presented.

In Figures 19 and 20, cesium concentrations as a function of ultrafiltration for long-term MgO hydration experiments in GWB are displayed. These experiments were conducted with large particle size MgO. Cesium concentrations are constant regardless of equivalent pore sizes, indicating the absence of mineral fragment colloids.

The results presented in Figures 21 and 22 are similar to those in Figures 19 and 20. The experiments presented in Figures 21 and 22 were conducted in GWB with mixed particle size MgO.

In Figure 23, the results from the long-term MgO hydration experiments in 1.0 $MgCl_2$ are presented. These experiments were conducted with large particle size MgO. The results are similar to those in Figures 19 and 20 in GWB.

In Figures 24 and 25, the results from the carbonation experiments conducted at $P_{CO_2} = 3.5 \times 10^{-4}$ atm with mixed particle size MgO in GWB are depicted. There is no dependence on equivalent pore size for cesium concentrations.

The results in Figures 26 through 28 are similar to those in Figures 24 and 25, except that the results in Figures 26 through 28 are from the carbonation experiments conducted at $P_{CO_2} = 3.5 \times 10^{-3}$ atm, which is one order of magnitude higher than that in Figures 24 and 25.

The results presented in Figure 29 are similar to those in Figures 26 through 28. The experiments in Figure 29 were with large particle size MgO, whereas those in Figures 26 through 28 were with mixed particle size MgO.

The results presented in Figure 30 are similar to those in Figure 29. The experiments in Figure 29 were with large particle size MgO in GWB, whereas those in Figure 30 were with mixed particle size MgO in simplified GWB.

In Figure 31, the results from the carbonation experiments conducted at $P_{CO_2} = 3.5 \times 10^{-3}$ atm with prehydrated large particle size MgO in GWB are depicted. As mentioned previously, MgO was prehydrated as brucite and phase 5. Therefore, these experiments investigated the direct carbonation of hydration products. These experimental results indicate that cesium concentrations remain constant regardless of ultrafiltration, suggesting the absence of mineral fragment colloids from both MgO hydration and carbonation products in GWB.

The results in Figure 32 are similar to those in Figure 31, except for that the carbonation experiments with prehydrated MgO in Figure 32 were conducted in simplified GWB.

In summary, the experimental results demonstrate that magnesium and cesium concentrations are independent of ultrafiltration, indicating the absence of mineral colloids associated with MgO hydration and carbonation processes. These experiments covered a wide range of conditions. In terms of MgO particle sizes, they included mixed (i.e., as-received) particle size MgO, large particle size MgO (i.e., 1 mm—2 mm), and small particle size MgO (i.e., < 75 μm). Regarding the solution medium, they included 1.0 $MgCl_2$, simplified GWB (1.0 M $MgCl_2$ + 3.6 M NaCl), GWB, and ERDA-6. With regard to the partial pressure of CO_2(g), they included $P_{CO_2} = 3.5 \times 10^{-4}$ atm and $P_{CO_2} = 3.5 \times 10^{-3}$ atm.

CONCLUSION

This work clearly demonstrates the absence of mineral fragment colloids in the SNL long-term MgO hydration and carbonation. This conclusion is reached based on two independent experimental approaches. The absence of mineral fragment colloids in the WIPP brines is due to the chemistry of the WIPP brines. The WIPP brines are characterized by high ionic strengths with GWB and ERDA-6 having ionic strengths of 8.26 mol•kg^{-1} and 5.82 mol•kg^{-1}, respectively (Xiong and Lord, 2008). Furthermore, these brines have high concentrations of both monovalent and divalent ions. The ERDA-6 brine has 5.35 mol•kg^{-1}, 0.106 mol•kg^{-1}, 0.0209 mol•kg^{-1}, 0.0132 mol•kg^{-1} for Na^+, K^+, Mg^{2+}, and Ca^{2+} (Xiong and Lord, 2008), respectively. GWB has 4.04 mol•kg^{-1}, 0.532 mol•kg^{-1}, 1.16 mol•kg^{-1}, 0.0163 mol•kg^{-1} for Na^+, K^+, Mg^{2+}, and Ca^{2+} (Xiong and Lord, 2008), respectively. These concentrations are much higher than the critical coagulation

concentrations. The direct consequence of the chemistry of the WIPP brines is that mineral fragment colloids that might be derived from MgO are unstable in these brines. The absence of mineral fragment colloids, as demonstrated experimentally by this study, obviously illustrates the role of the WIPP brine chemistry in destabilization of mineral fragment colloids.

The absence of MgO hydration and carbonation product mineral fragment colloids in the brines associated with salt formations, as indicated by this work, has important implications to disposal of nuclear waste in salt formations. The high ionic strength brines associated with salt formations provide favorable near-field geochemical conditions that will de-stabilize mineral fragment colloids. The absence of colloids of any kind is a favorable result for the performance of a nuclear waste repository in salt formations.

ACKNOWLEDGEMENTS

Sandia National Laboratories is a multimission laboratory managed and operated by National Technology and Engineering Solutions of Sandia, LLC., a wholly owned subsidiary of Honeywell International, Inc., for the U.S. Department of Energy's National Nuclear Security Administration under contract DE-NA-0003525. SAND2017-XXXX. This research is funded by the WIPP programs administered by the Office of Environmental Management (EM) of the U.S. Department of Energy.

REFERENCES

Allen, L.H. and E. Matijević, 1969. "Stability of colloidal silica: I. Effect of simple electrolytes." *Journal of Colloid and Interface Science* 31:287-296.

Allen, L.H. and E. Matijevic, 1971. "Stability of colloidal silica: II. Ion exchange." *Journal of Colloid and Interface Science* 33:420–429.

Altmaier, M., V. Neck, and Th. Fanghanel, 2004. "Solubility and colloid formation of Th(IV) in concentrated NaCl and $MgCl_2$ solution." *Radiochimica Acta* 92:537–543.

Apalkov, Gleb, Alexander Dyachenko, Andrey Zhabin, and Sergey Smirnov, 2016. "Development of a purification technology for treatment of medium-

and low-activity radioactive waste of radiochemical production from Co-60 and Cs-137." *MATEC Web of Conferences* 85:01021. EDP Sciences.

Bascetin, E., H. Haznedaroglu, and A. Y. Erkol, 2003. "The adsorption behavior of cesium on silica gel." *Applied radiation and isotopes 59*:5-9.

Bitea, C., C. Walther, J.-I Kim, H. Geckeis, T. Rabung, F.J. Scherbaum, D. G. Cacuci, 2003. "Time-resolved observation of ZrO_2-colloid agglomeration." *Colloids and Surfaces A: Physicochem. Eng. Aspects* 215:55–66.

Chen, G., M, Flury, J.B. Harsh, and P.C. Lichtner, 2005. "Colloid-facilitated transport of cesium in variably saturated Hanford sediments." *Environmental science & technology* 39:3435-3442.

Cheng, Tao, and James E. Saiers, 2010. "Colloid-facilitated transport of cesium in vadose-zone sediments: the importance of flow transients." *Environmental Science & Technology* 44:7443–7449.

Cheng, Tao, and James E. Saiers. 2015. "Effects of dissolved organic matter on the co-transport of mineral colloids and sorptive contaminants." *Journal of contaminant hydrology* 177:148–157.

Deng, H.-R., Nemer, M., and Xiong, Y.-L., 2006. "Test Plan TP 06-03 Experimental Study of MgO Reaction Pathways and Kinetics, Revision 1." Sandia National Laboratories, Carlsbad, NM.

Deng, Haoran, Yongliang Xiong, Martin Nemer, and Shelly Johnsen, 2008. "Experimental Work Conducted on MgO Characterization and Hydration." *MRS Proceedings*1124: 1124-Q05. Cambridge University Press.

Deng, H.-R., Y.-L. Xiong, M. Nemer, and S. Johnsen, 2009. "Experimental work conducted on MgO long-term hydration, 2008 Milestone Report." Sandia National Laboratories, Carlsbad, NM, ERMS 551421.

Itagaki, H., S. Tanaka, M. Yamawaki, 1991. "Neptunium chemical behavior in underground environments using ultrafiltration and centrifugation." Radiochimica Acta 52/53:91–94.

Kelly, J.W., R. Aguilar, and H.W. Papenguth, 1996. "Contribution of mineral-fragment type pseudo-colloids to the mobile actinide source term of the Waste Isolation Pilot Plant (WIPP)." Sandia National Laboratories, Albuquerque, NM, SAND96-2742J.

Kim, Intae, and Guebuem Kim, 2015. "Role of colloids in the discharge of trace elements and rare earth elements from coastal groundwater to the ocean." *Marine Chemistry* 176:126–132.

Kim, J. I., B. Delakowitz, P. Zeh, D. Klotz, D. Lazik, 1994. "A column experiment for the study of colloidal radionuclide migration in Gorleben aquifer systems." *Radiochimica Acta* 66/67:165–171.

Olofsson, U., and B. Allard, 1986. "Formation and transport of americium pseudocolloids in aqueous systems." SKBF/KBS Technical Report -TR 86-02, Swedish Nucl. Fuel and Waste Management Co., Stockholm.

Olofsson, U., B. Allard, M. Bengtsson, B. Torstenfelt, K. Andersson, 1983. "Formation and Properties of Actinide Colloids." SKBF/KBS Technical Report -TR 83-08, Swedish Nucl. Fuel and Waste Management Co., Stockholm.

Ross, J.M. and R.M. Sherrell, 1999. "The role of colloids in trace metal transport and adsorption behavior in New Jersey Pinelands streams." *Limnol. Oceanogr* 44:1019–1034.

Sasaki, Takayuki, Yuu Takeno, Akira Kirishima, and Nobuaki Sato, 2015. "Leaching test of gamma-emitting Cs, Ru, Zr, and U from neutron-irradiated UO_2/ZrO_2 solid solutions in non-filtered surface seawater: Fukushima NPP Accident Related." *Journal of Nuclear Science and Technology* 52:147–151.

Savenko, A. V., N. A. Demidenko, and O. S. Pokrovskii, 2016. "Chemical transformation of the runoff of dissolved matters in the mouth areas of the Onega and Mezen'rivers." *Geochemistry International* 54:439-448.

Schuessler, W., B. Kienzler, S. Wilhelm, V. Neck, and J.I. Kim, 2001. "Modeling of Near Field Actinide Concentrations in Radioactive Waste Repositories in Salt Formations: Effect of Buffer Materials." *Mat. Res. Soc. Symp. Proc.* 663:791.

Silva, R.J., H. Nitsche, 1995. "Actinide environmental chemistry." *Radiochimica Acta* 70/71:377–396.

U.S. National Academy of Sciences Committee on Waste Disposal. 1957. *The Disposal of Radioactive Waste on Land.* Publication 519. Washington, DC: National Academy of Sciences–National Research Council.

van Olphen, H. 1991. "An Introduction to Clay Colloid Chemistry: For Clay Technologists, Geologists, and Soil Scientists." 2nd ed. Malabar, FL: Krieger Pub. Co. (Reprint of 1977- 2nd edition originally published by John Wiley& Sons.).

Wang, Dengjun, Yan Jin, and Deb P. Jaisi, 2015. "Cotransport of hydroxyapatite nanoparticles and hematite colloids in saturated porous media: Mechanistic insights from mathematical modeling and phosphate oxygen isotope fractionation." *Journal of contaminant hydrology* 182:194–209.

Wen, L. S., Santschi, P. H., Paternostro, C. and Gill, G., 1999. "Estuarine trace metal distributions in Galveston Bay I: importance of colloidal forms in the speciation of the dissolved phase." *Mar. Chem* 63:185–212.

Xiong, Y.-L., 2008. "SP 20-4, Preparing Synthetic Brines for Geochemical Experiments, Revision 2." Sandia National Laboratories, Carlsbad, NM.

Xiong, Y.-L., and A.C.S. Lord, 2008. "Experimental investigations of the reaction path in the $MgO–CO_2–H_2O$ system in solutions with ionic strengths, and their applications to nuclear waste isolation." *Applied Geochemistry* 23:1634–1659.

Xiong, Y.-L., L.H. Brush, J. Garner, and J.J Long, 2010a. "Responses to three EPA comments pertaining to comparisons of measured and predicted dissolved and colloidal Th(IV) and Am(III) concentrations, Revision 1." Supersedes ERMS 553409. Sandia National Laboratories, Carlsbad, NM, ERMS 553595

Xiong, Y.-L., H. Deng, M. Nemer, S. Johnsen, 2010b. "Experimental determination of the solubility constant for magnesium chloride hydroxide hydrate ($Mg_3Cl(OH)_5•4H_2O$, phase 5) at room temperature, and its importance to nuclear waste isolation in geological repositories in salt formations." *Geochimica et Cosmochimica Acta* 74:4605–4611.

Zhao, P.-H., S.S. Steward, 1997. "Literature review of intrinsic colloids related to spent fuel waste package release rates." Lawrence Livermore National Laboratory, UCRL-ID-126039.

Table 1. Recipes for Synthetic Salado and Castile Brines on Molarity Scale (from Xiong, 2008)

Salt	GWB	ERDA-6
	Grams for1L	Grams for 1L
$Na_2B_4O_7 \cdot 10H_2O$	15.06	6.00
NaBr	2.74	1.13
LiCl	0.19	None
NaCl	179.61	261.64
KCl	34.84	7.23
$MgCl_2 \cdot 6H_2O$	207.05	3.86
$CaCl_2 \cdot 2H_2O$	2.03	1.76
Na_2SO_4	25.23	23.70

Table 2. Recipes for Synthetic Salado and Castile Brines on Molality Scale (from Xiong, 2008)

Salt	GWB Grams for 1,000 g H_2O	ERDA-6 Grams for 1,000 g H_2O
$Na_2B_4O_7 \cdot 10H_2O$	16.96	6.73
NaBr	3.09	1.27
LiCl	0.21	None
NaCl	202.32	293.38
KCl	39.25	8.11
$MgCl_2 \cdot 6H_2O$	233.23	4.33
$CaCl_2 \cdot 2H_2O$	2.29	1.97
Na_2SO_4	28.42	26.58

Figure Captions

Figure 1. Magnesium concentrations in solution samples from MgO hydration experiments in GWB with large particle size MgO as a function of equivalent pore size. The experiments include GW20L28, GW20L33 through GW20L36. In each experiment, there was 3.1 g of MgO with 77 mL of GWB.

Figure 2. Magnesium concentrations in solution samples from MgO hydration experiments in GWB with large particle size MgO as a function of equivalent pore size. The experiments include GW20L19 through GW20L23, and GW20L27. In each experiment, there was 3.1 g of MgO with 77 mL of GWB.

Figure 3. Magnesium concentrations in solution samples from MgO hydration experiments in a 1.0 M $MgCl_2$ solution with large particle size MgO and mixed size MgO as a function of equivalent pore size. The experiments with large particle size MgO include (MgCl2)20L27 through (MgCl2)20L28. In each above experiment, there was 3.1 g of MgO with 77 mL of 1.0 M $MgCl_2$. The experiments with mixed size MgO include (MgCl2)3M25 through (MgCl2)3M27. In each experiment with mixed size MgO, there was 3 g of MgO with 11 mL of1.0 M $MgCl_2$.

Figure 4. Magnesium concentrations in solution samples from MgO hydration experiments in a 1.0 M $MgCl_2$ solution with small particle size MgO and mixed size MgO as a function of equivalent pore size. The experiments with small particle size MgO include (MgCl2)3S27 through (MgCl2)3S28. In each above experiment, there was 3 g of MgO with 11 mL of 1.0 M $MgCl_2$. The experiments with mixed size MgO include (MgCl2)20M27 through (MgCl2)20M28. In each experiment with mixed size MgO, there was 3.1 g of MgO with 77 mL of1.0 M $MgCl_2$.

Figure 5. Magnesium concentrations in solution samples from MgO carbonation experiments in GWB with mixed particle size MgO at $P_{CO_2} = 3.5 \times 10^{-4}$ atm, as a function of equivalent pore size. The experiments include 1:20GWBA5 through 1:20GWBA9. In each experiment, there was 3.1 g of MgO with 77 mL of GWB.

Figure 6. Magnesium concentrations in solution samples from MgO carbonation experiments in GWB with mixed particle size MgO at $P_{CO_2} = 3.5 \times 10^{-4}$ atm, as a function of equivalent pore size. The experiments include 1:20GWBA10 through 1:20GWBA14. In each experiment, there was 3.1 g of MgO with 77 mL of GWB.

Figure 7. Magnesium concentrations in solution samples from MgO carbonation experiments in GWB with mixed particle size MgO at $P_{CO_2} = 3.5 \times 10^{-3}$ atm, as a function of equivalent pore size. The experiments include 1:20GWBB7 through 1:20GWBB13. In each experiment, there was 3.1 g of MgO with 77 mL of GWB.

Figure 8. Magnesium concentrations in solution samples from MgO carbonation experiments in GWB with mixed particle size MgO at $P_{CO_2} = 3.5 \times 10^{-3}$ atm, as a function of equivalent pore size. The experiments include 1:20GWBB14 through 1:20GWBB20. In each experiment, there was 3.1 g of MgO with 77 mL of GWB.

Figure 9. Magnesium concentrations in solution samples from MgO carbonation experiments in GWB with mixed particle size MgO at $P_{CO_2} = 3.5 \times 10^{-3}$ atm, as a function of equivalent pore size. The experiments include 1:20GWBB21 through 1:20GWBB28. In each experiment, there was 3.1 g of MgO with 77 mL of GWB.

Figure 10. Magnesium concentrations in solution samples from MgO carbonation experiments in GWB with large particle size MgO at $P_{CO_2} = 3.5 \times 10^{-3}$ atm, as a function of equivalent pore size. The experiments include 1:20GWBD5 through 1:20GWBD12. In each experiment, there was 3.1 g of MgO with 77 mL of GWB.

Figure 11. Magnesium concentrations in solution samples from MgO carbonation experiments in GWB with large particle size MgO at $P_{CO_2} = 3.5 \times 10^{-3}$ atm, as a function of equivalent pore size. The experiments include 1:20GWBD13 through 1:20GWBD20. In each experiment, there was 3.1 g of MgO with 77 mL of GWB.

Figure 12. Magnesium concentrations in solution samples from MgO carbonation experiments in GWB with large particle size MgO at $P_{CO_2} = 3.5 \times 10^{-3}$ atm, as a function of equivalent pore size. The experiments include 1:20GWBD21 through 1:20GWBD28. In each experiment, there was 3.1 g of MgO with 77 mL of GWB.

Figure 13. Magnesium concentrations in solution samples from MgO carbonation experiments in simplified GWB with mixed particle size MgO at $P_{CO_2} = 3.5 \times 10^{-3}$ atm, as a function of equivalent pore size. The experiments include 1:20SGWB22 through 1:20SGWB24. In each experiment, there was 3.1 g of MgO with 77 mL of simplified GWB.

Figure 14. Magnesium concentrations in solution samples from MgO carbonation experiments in simplified GWB with mixed particle size MgO at $P_{CO_2} = 3.5 \times 10^{-3}$ atm, as a function of equivalent pore size. The experiments include 1:20SGWB15 through 1:20SGWB16, 1:20SGWB18 through 1:20SGWB21. In each experiment, there was 3.1 g of MgO with 77 mL of simplified GWB.

Figure 15. Magnesium concentrations in solution samples from MgO carbonation experiments in GWB with prehydrated mixed particle size MgO at $P_{CO_2} = 3.5 \times 10^{-4}$ atm, as a function of equivalent pore size. The experiments include 1:20GWBMgOHA7 through 1:20GWBMgOHA14. In each experiment, there was 3.1 g of MgO with 77 mL of GWB.

Figure 16. Magnesium concentrations in solution samples from MgO carbonation experiments in simplified GWB with prehydrated mixed particle size MgO at $P_{CO_2} = 3.5 \times 10^{-3}$ atm, as a function of equivalent pore size. The experiments include 1:20SGWBMgOHB7 through 1:20GWBMgOHB14. In each experiment, there was 3.1 g of MgO with 77 mL of simplified GWB.

Figure 17. Magnesium concentrations in solution samples from MgO carbonation experiments in ERDA-6 with small particle size MgO at $P_{CO_2} = 3.5 \times 10^{-3}$ atm, as a function of equivalent pore size. The experiments include 1:20ERC-9 through 1:20ERC-14. In each experiment, there was 3.1 g of MgO with 77 mL of ERDA-6.

Figure 18. Magnesium concentrations in solution samples from MgO carbonation experiments in ERDA-6 with small particle size MgO at $P_{CO_2} = 3.5 \times 10^{-3}$ atm, as a function of equivalent pore size. The experiments include 1:20ERC-15 through 1:20ERC-28. In each experiment, there was 3.1 g of MgO with 77 mL of ERDA-6.

Figure 19. Cesium concentrations in solution samples from MgO hydration experiments in GWB with large particle size MgO as a function of equivalent pore size. The experiments include GW20L19 through GW20L25. In each experiment, there was 3.1 g of MgO with 77 mL of GWB.

Figure 20. Cesium concentrations in solution samples from MgO hydration experiments in GWB with large particle size MgO as a function of equivalent pore size. The experiments include GW20L26 through GW20L28, GW20L33 through GW20l35. In each experiment, there was 3.1 g of MgO with 77 mL of GWB.

Figure 21. Cesium concentrations in solution samples from MgO hydration experiments in GWB with mixed particle size MgO as a function of equivalent pore size. The experiments include GW20M19 through GW20M26. In each experiment, there was 3.1 g of MgO with 77 mL of GWB.

Figure 22. Cesium concentrations in solution samples from MgO hydration experiments in GWB with mixed particle size MgO as a function of equivalent pore size. The experiments include GW20M27 through GW20M28, GW20M31 through GW20M36. In each experiment, there was 3.1 g of MgO with 77 mL of GWB.

Figure 23. Cesium concentrations in solution samples from MgO hydration experiments in 1.0 M $MgCl_2$ with mixed and large particle size MgO as a function of equivalent pore size. The experiments with mixed particle size MgO include MgCl2-20M27 and MgCl2-20M28. The experiments with large particle size MgO include MgCl2-20L27 and MgCl2-20L28. In each experiment, there was 3.1 g of MgO with 77 mL of 1.0 M $MgCl_2$.

Figure 24. Cesium concentrations in solution samples from MgO carbonation experiments in GWB with mixed particle size MgO at $P_{CO_2} = 3.5 \times 10^{-4}$ atm, as a function of equivalent pore size. The experiments include 1:20GWBA5 through 1:20GWBA9. In each experiment, there was 3.1 g of MgO with 77 mL of GWB.

Figure 25. Cesium concentrations in solution samples from MgO carbonation experiments in GWB with mixed particle size MgO at $P_{CO_2} = 3.5 \times 10^{-4}$ atm, as a function of equivalent pore size. The experiments include 1:20GWBA10 through 1:20GWBA14. In each experiment, there was 3.1 g of MgO with 77 mL of GWB.

Figure 26. Cesium concentrations in solution samples from MgO carbonation experiments in GWB with mixed particle size MgO at $P_{CO_2} = 3.5 \times 10^{-3}$ atm, as a function of equivalent pore size. The experiments include 1:20GWBB7 through 1:20GWBB13. In each experiment, there was 3.1 g of MgO with 77 mL of GWB.

Figure 27. Cesium concentrations in solution samples from MgO carbonation experiments in GWB with mixed particle size MgO at $P_{CO_2} = 3.5 \times 10^{-3}$ atm, as a function of equivalent pore size. The experiments include 1:20GWBB14 through 1:20GWBB20. In each experiment, there was 3.1 g of MgO with 77 mL of GWB.

Figure 28. Cesium concentrations in solution samples from MgO carbonation experiments in GWB with mixed particle size MgO at $P_{CO_2} = 3.5 \times 10^{-3}$ atm, as a function of equivalent pore size. The experiments include 1:20GWBB21 through 1:20GWBB28. In each experiment, there was 3.1 g of MgO with 77 mL of GWB.

Figure 29. Cesium concentrations in solution samples from MgO carbonation experiments in GWB with large particle size MgO at $P_{CO_2} = 3.5 \times 10^{-3}$ atm, as a function of equivalent pore size. The experiments include 1:20GWBD13 through 1:20GWBD20. In each experiment, there was 3.1 g of MgO with 77 mL of GWB.

Figure 30. Cesium concentrations in solution samples from MgO carbonation experiments in simplified GWB with mixed particle size MgO at $P_{CO_2} = 3.5 \times 10^{-3}$ atm, as a function of equivalent pore size. The experiments include 1:20SGWBB15 through 1:20SGWBB21. In each experiment, there was 3.1 g of MgO with 77 mL of simplified GWB.

Figure 31. Cesium concentrations in solution samples from MgO carbonation experiments in GWB with prehydrated large particle size MgO at $P_{CO_2} = 3.5 \times 10^{-3}$ atm, as a function of equivalent pore size. The experiments include 1:20GWBMgOHA7 through 1:20GWBMgOHA13. In each experiment, there was 3.1 g of MgO with 77 mL of GWB.

Figure 32. Cesium concentrations in solution samples from MgO carbonation experiments in simplified GWB with prehydrated large particle size MgO at $P_{CO_2} = 3.5 \times 10^{-3}$ atm, as a function of equivalent pore size. The experiments include 1:20SGWBMgOHB7 through 1:20SGWBMgOHB14. In each experiment, there was 3.1 g of MgO with 77 mL of simplified GWB.

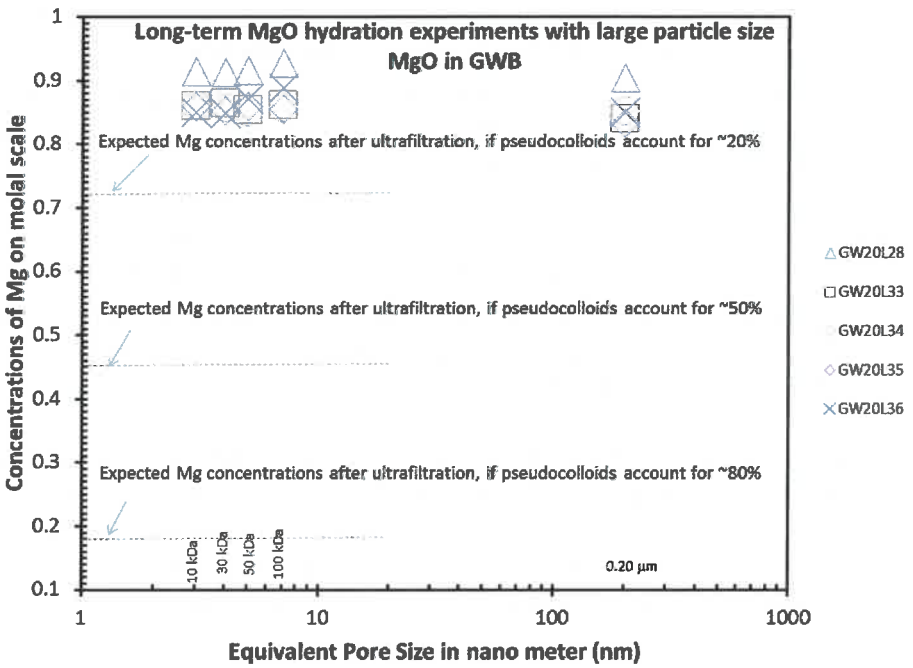

Figure 1

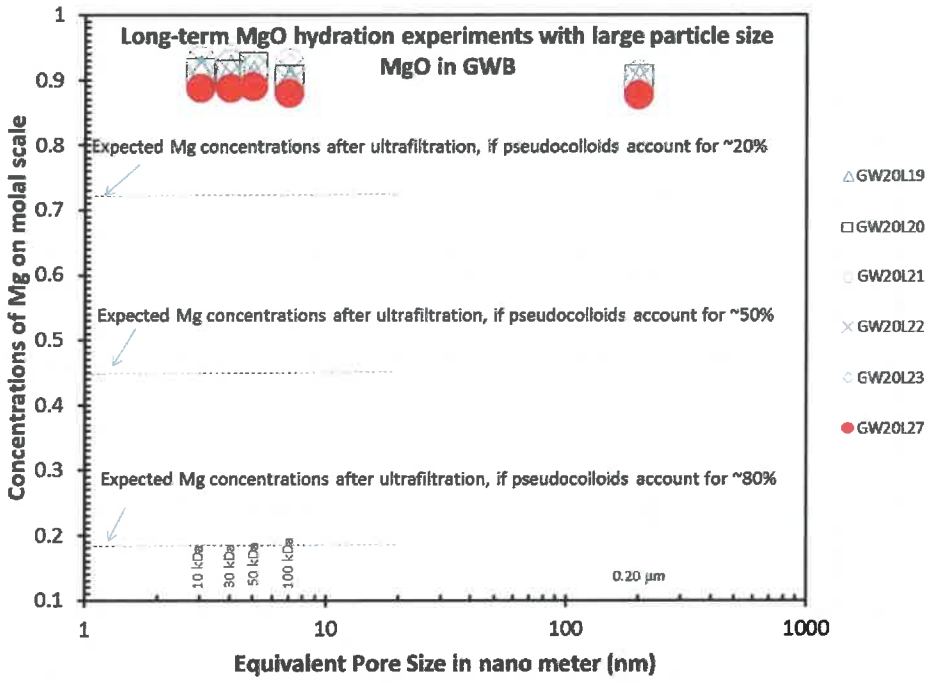

Figure 2

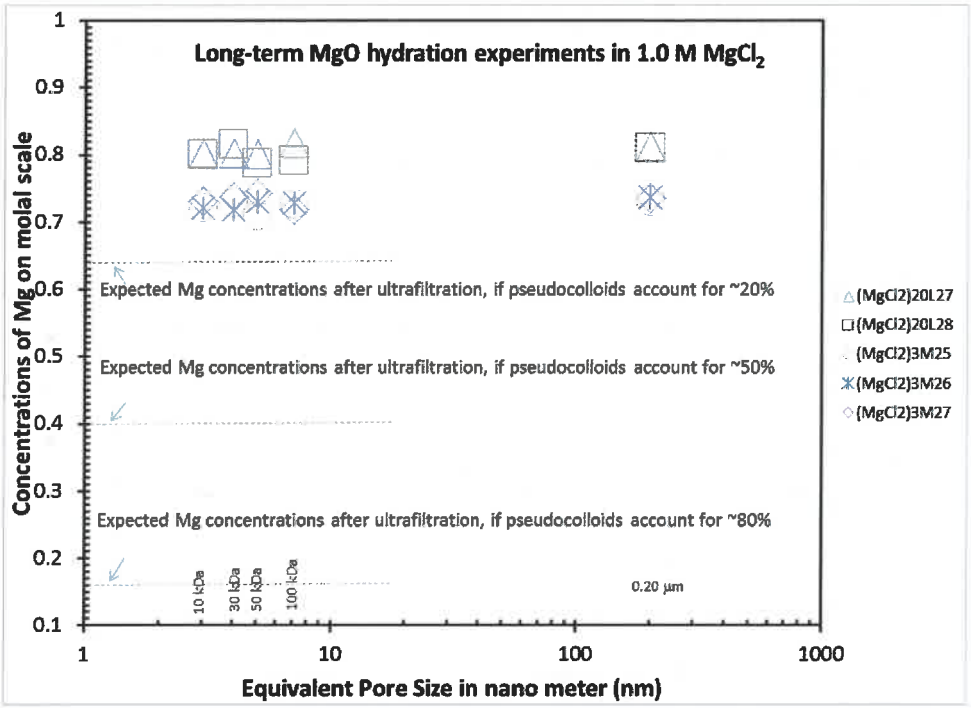

Figure 3

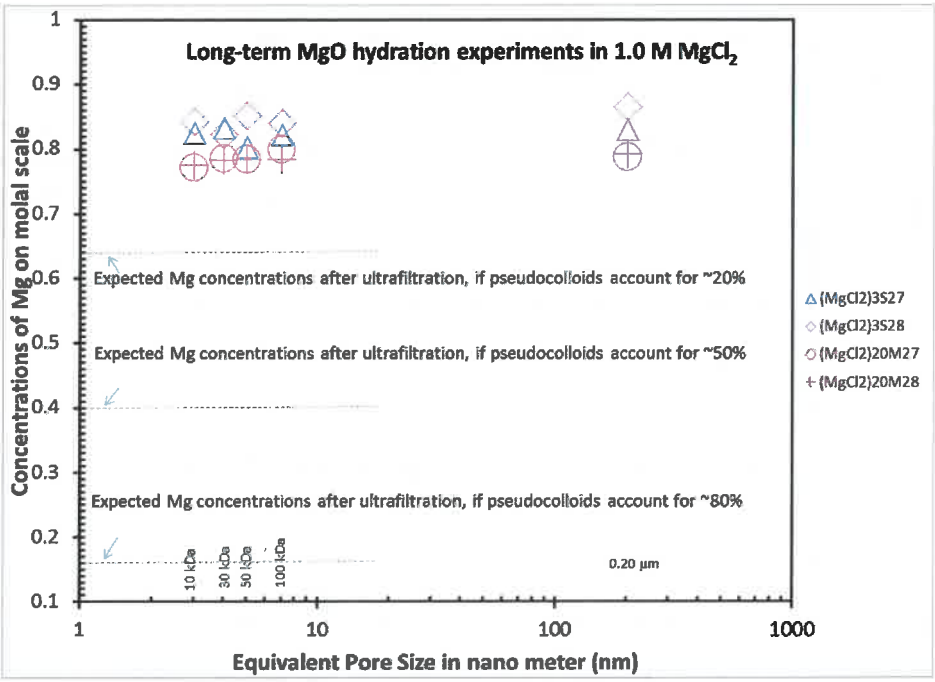

Figure 4

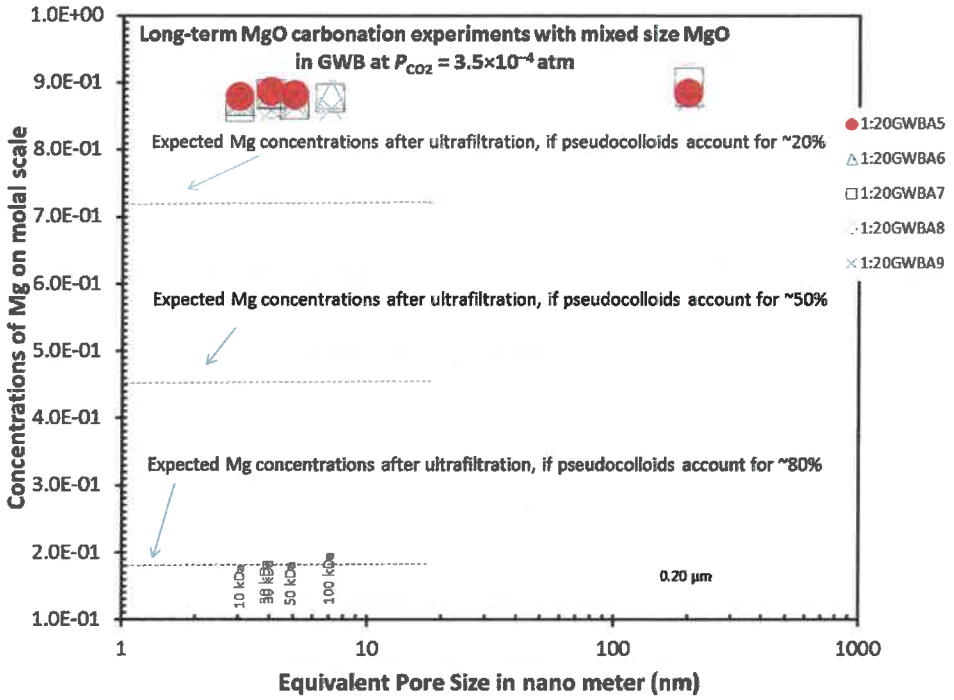

Figure 5

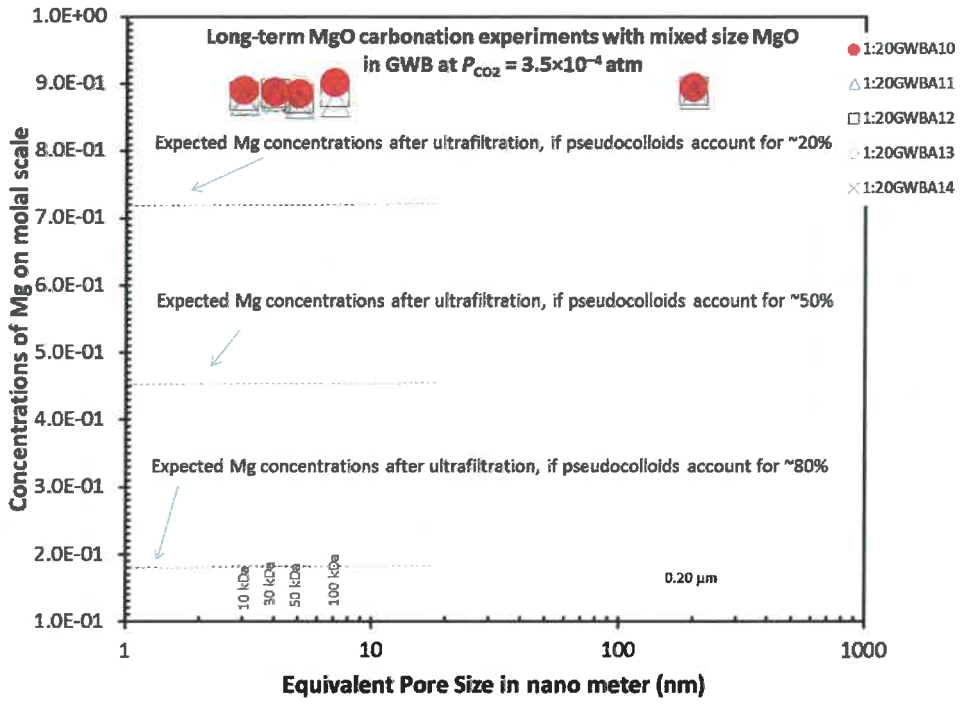

Figure 6

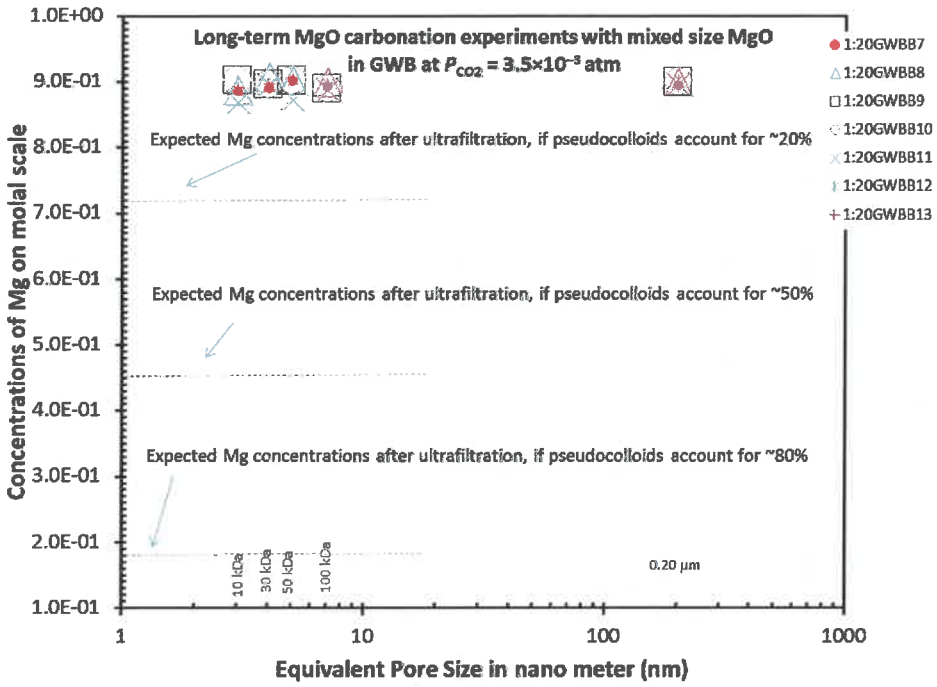

Figure 7

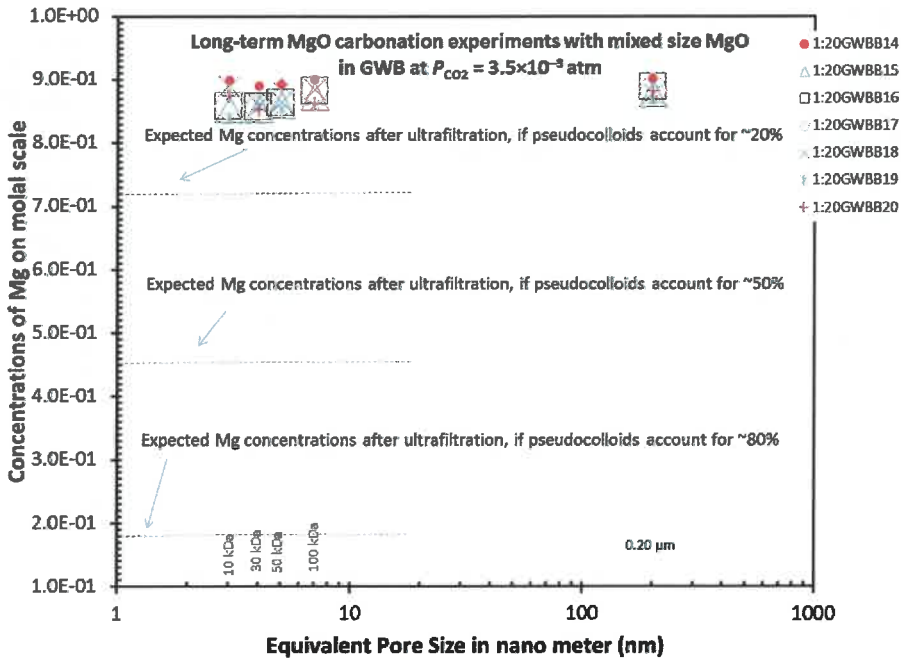

Figure 8

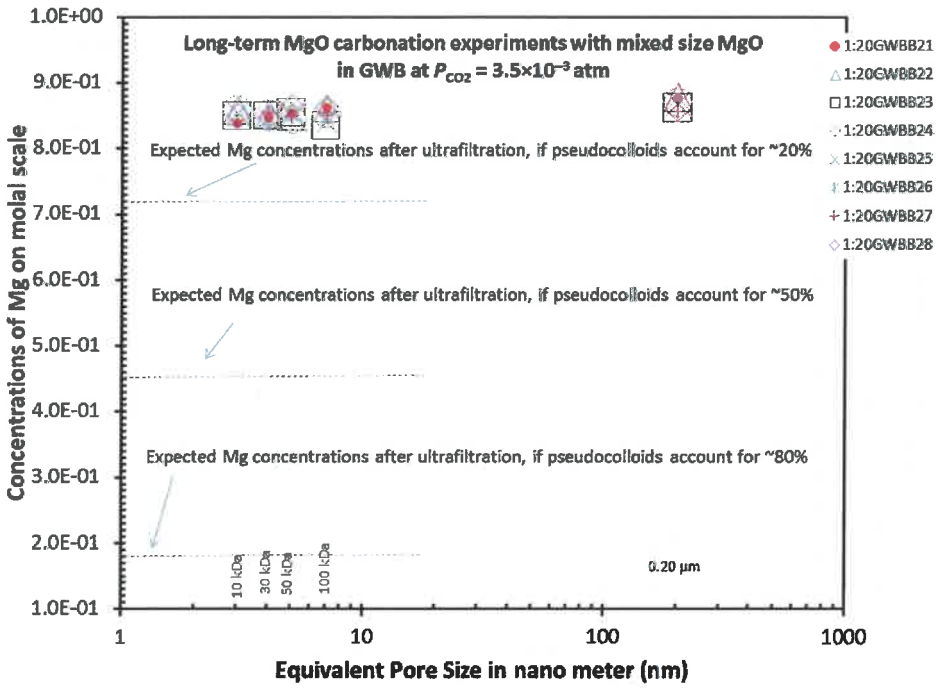

Figure 9

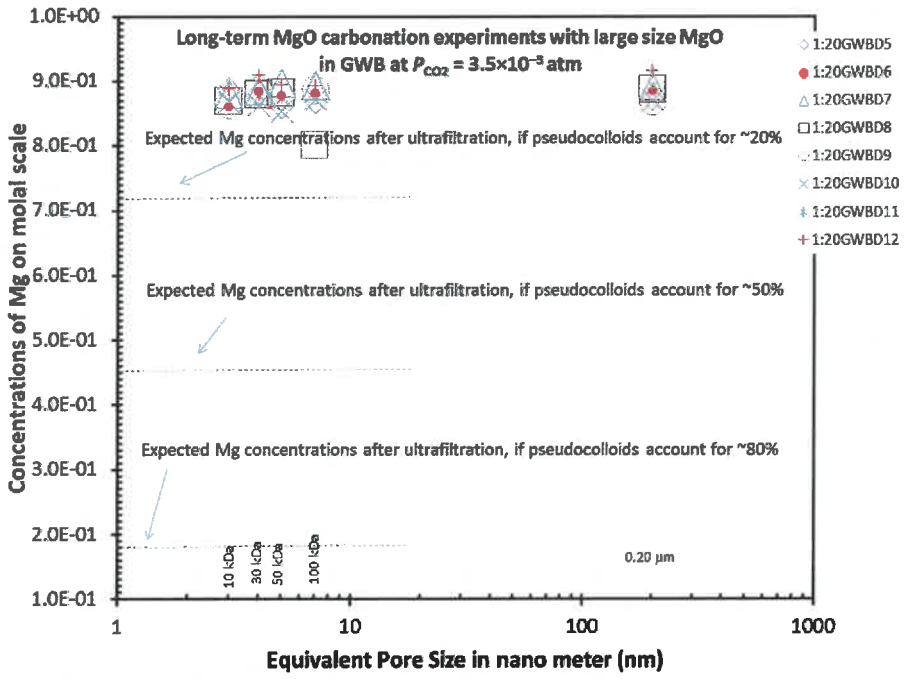

Figure 10

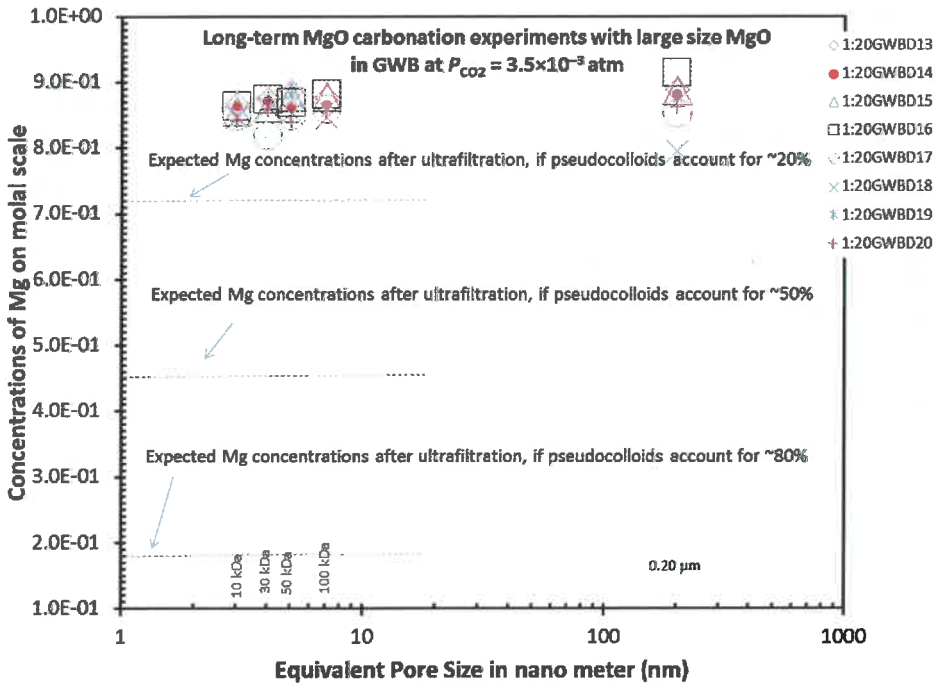

Figure 11

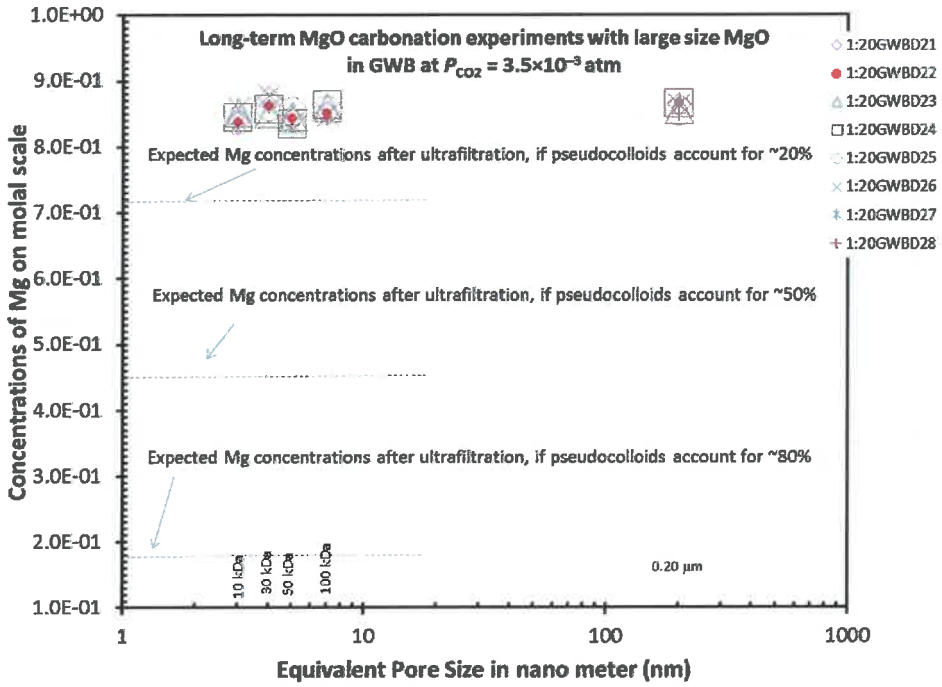

Figure 12

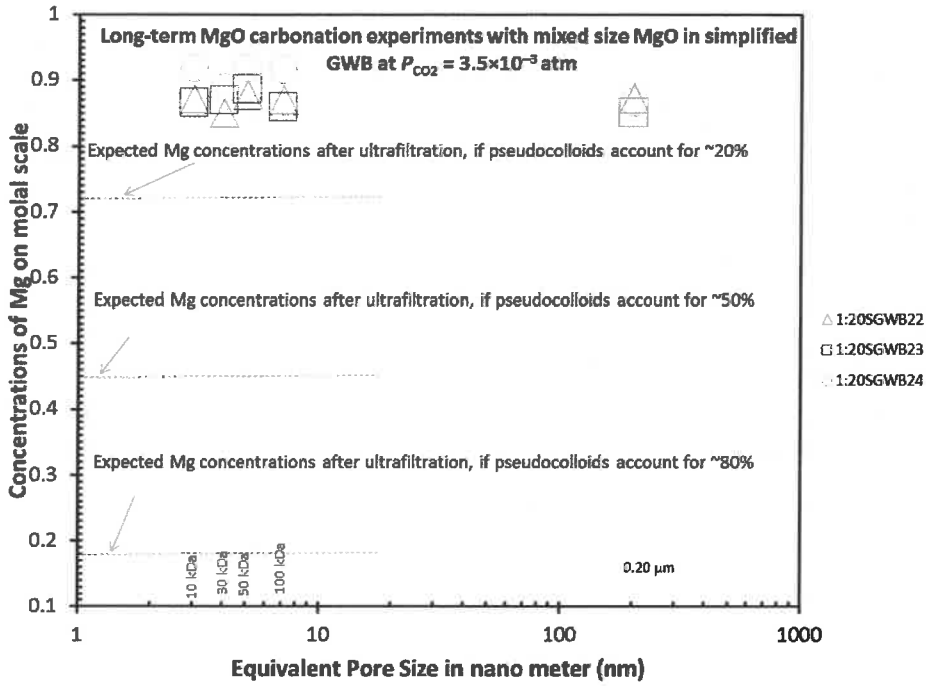

Figure 13

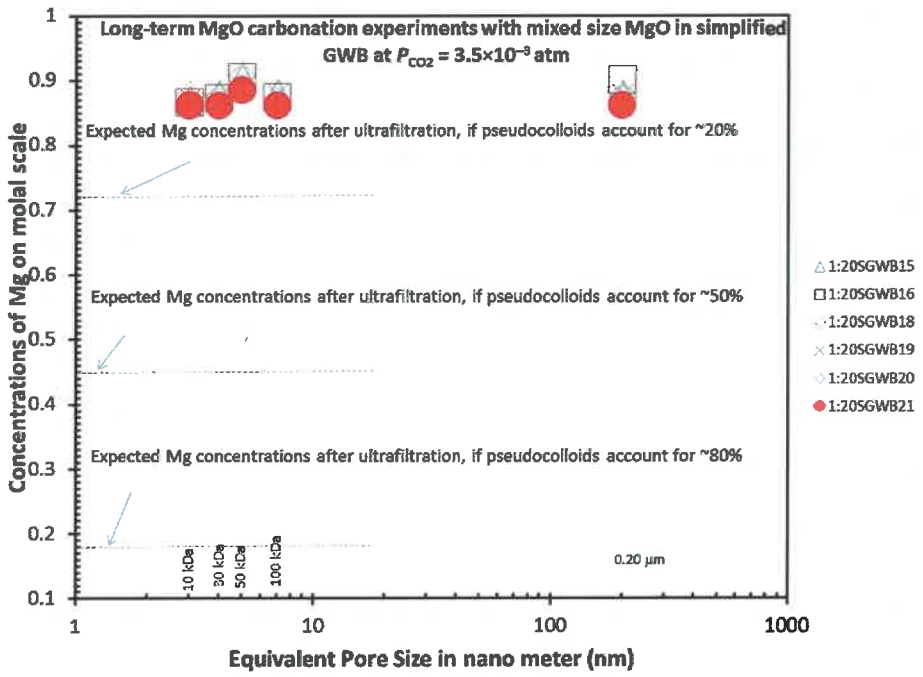

Figure 14

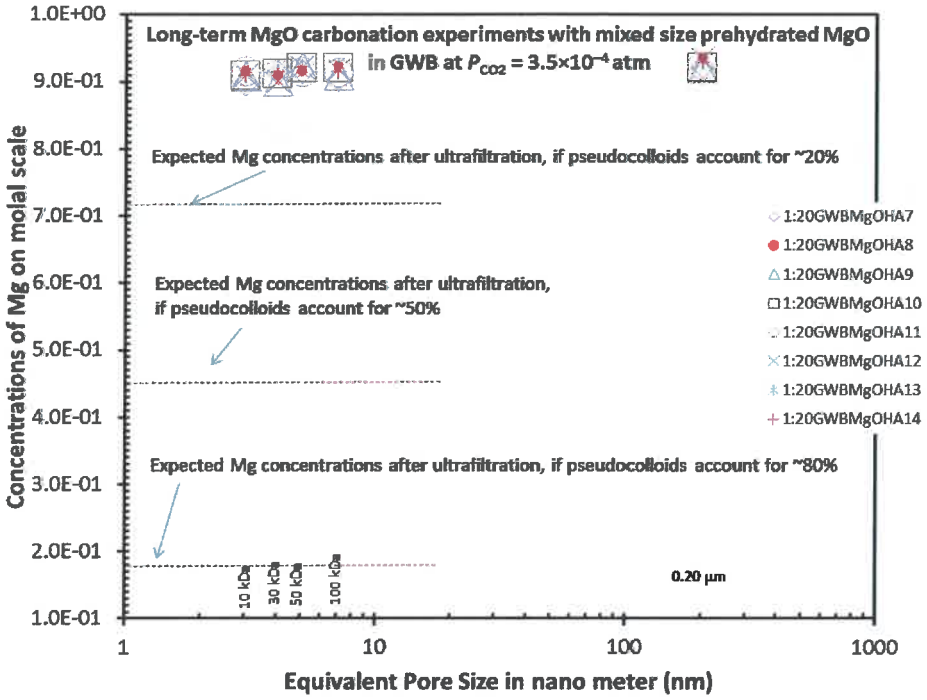

Figure 15

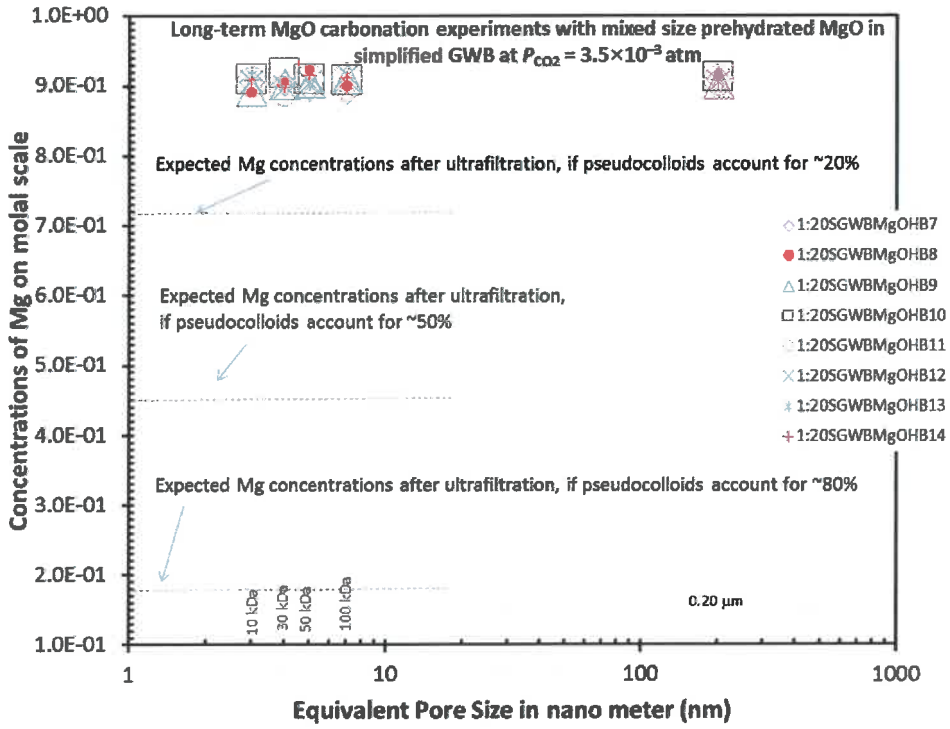

Figure 16

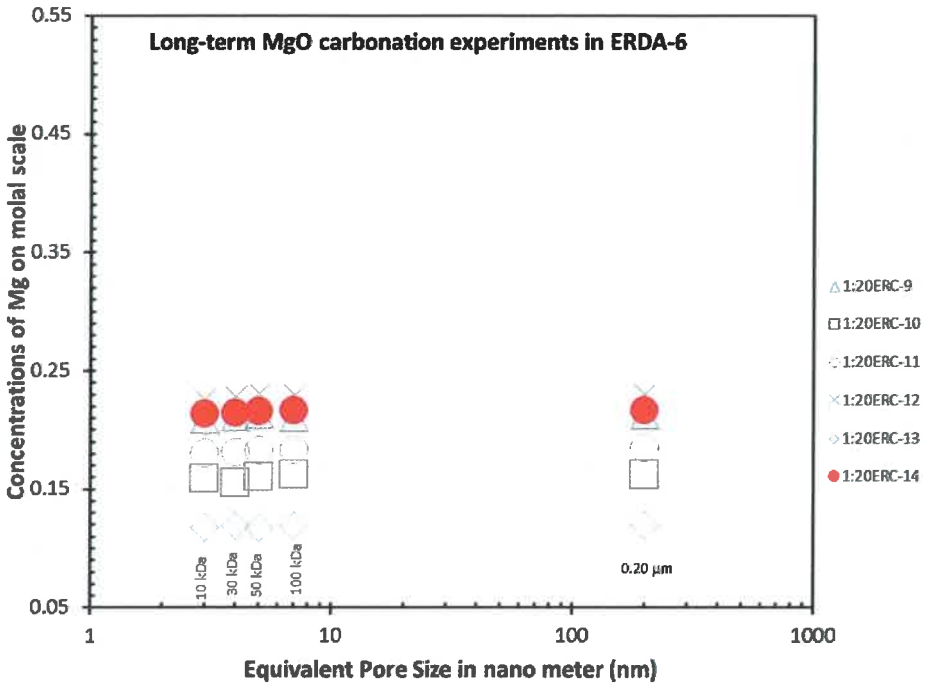

Figure 17.

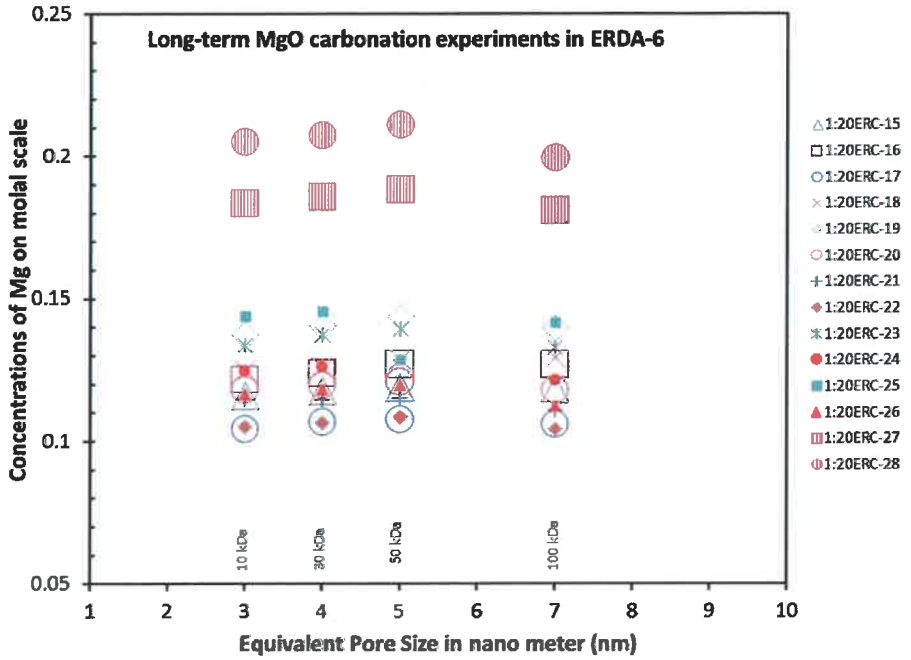

Figure 18.

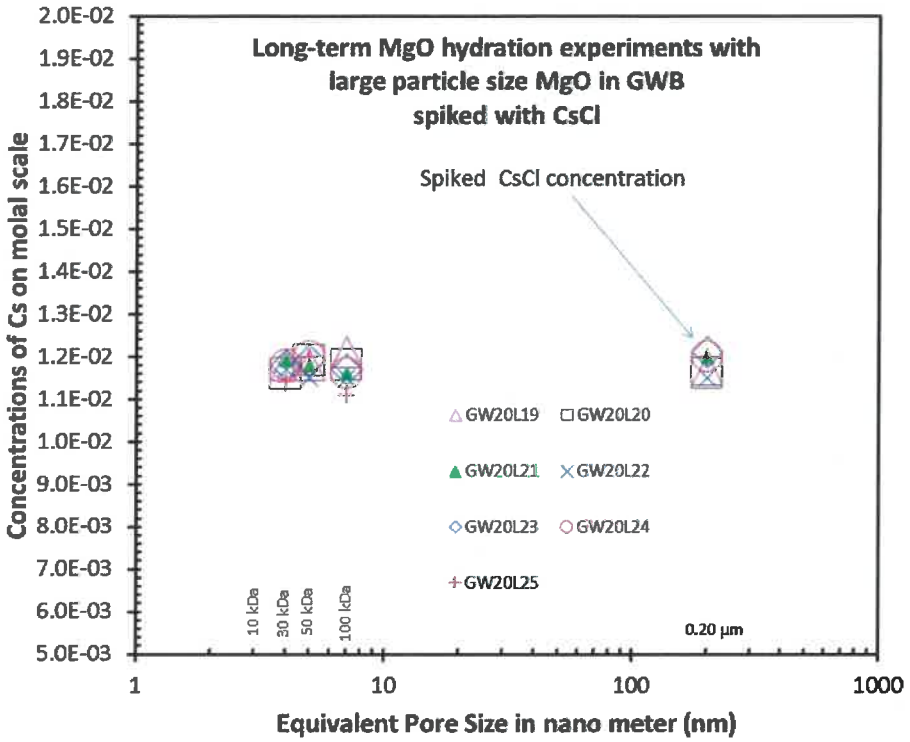

Figure 19

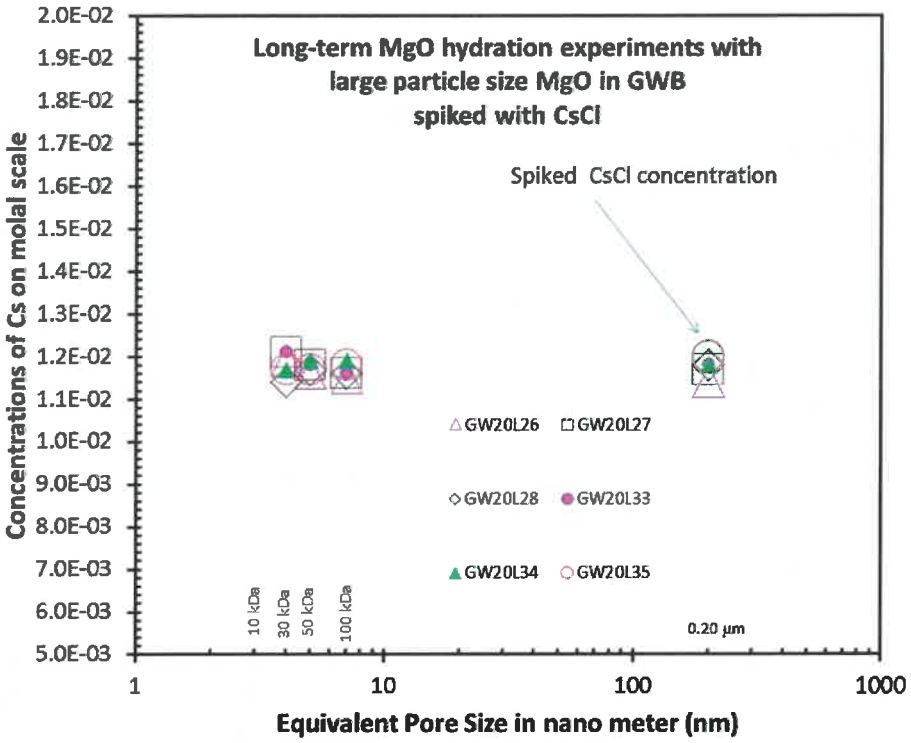

Figure 20

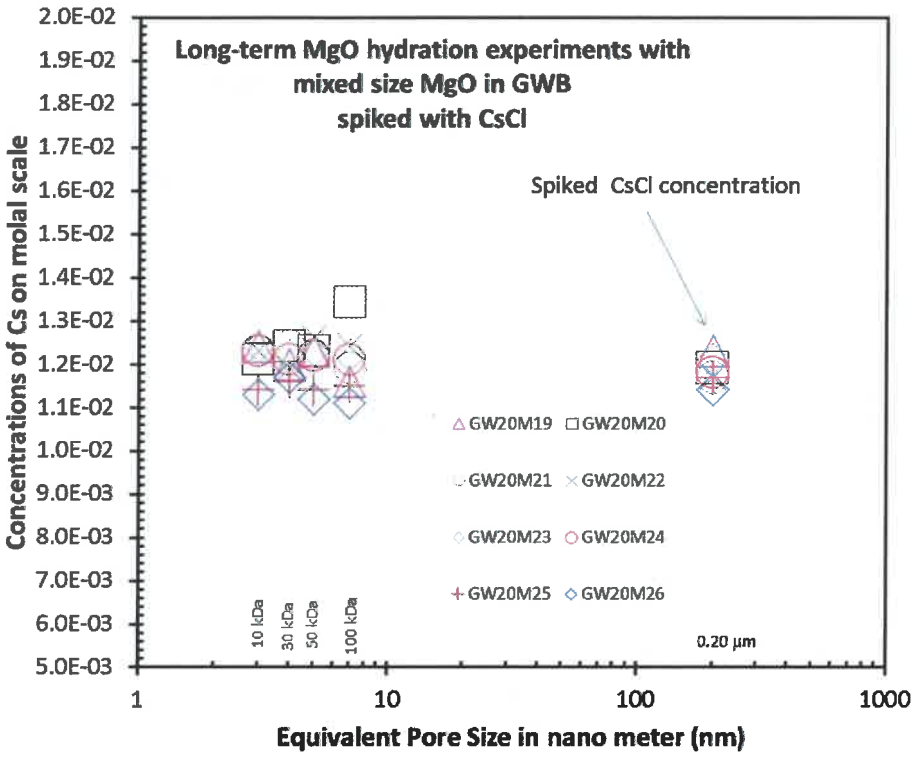

Figure 21

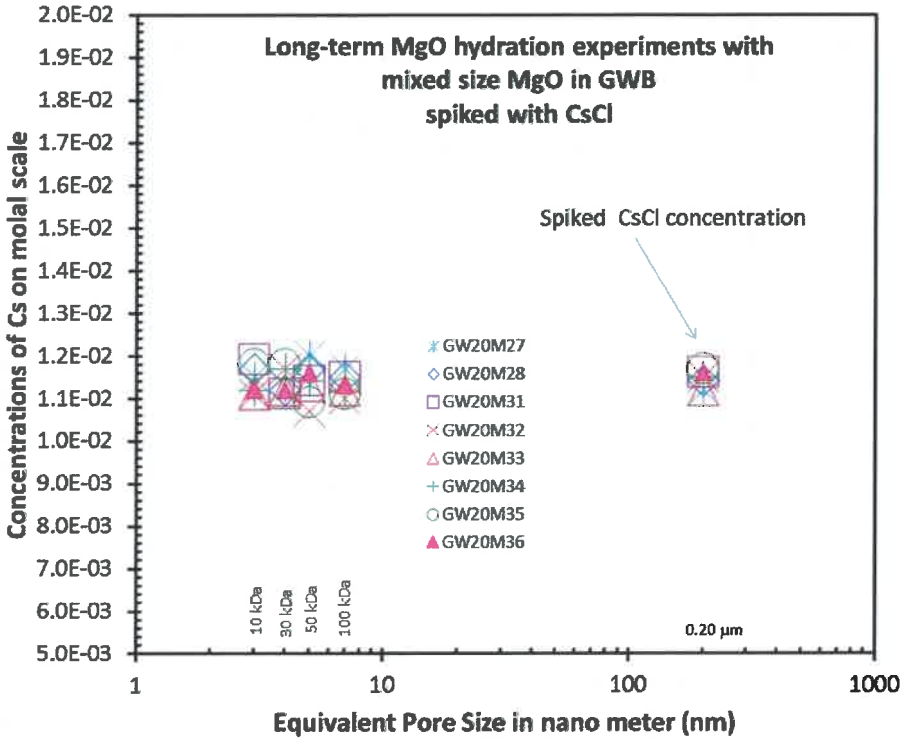

Figure 22

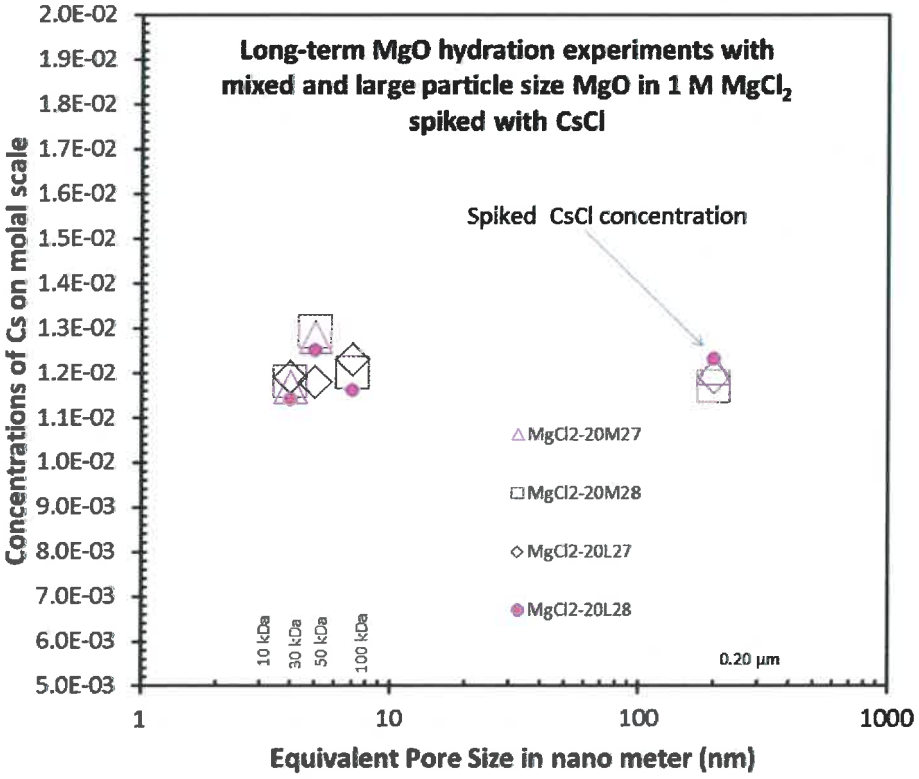

Figure 23

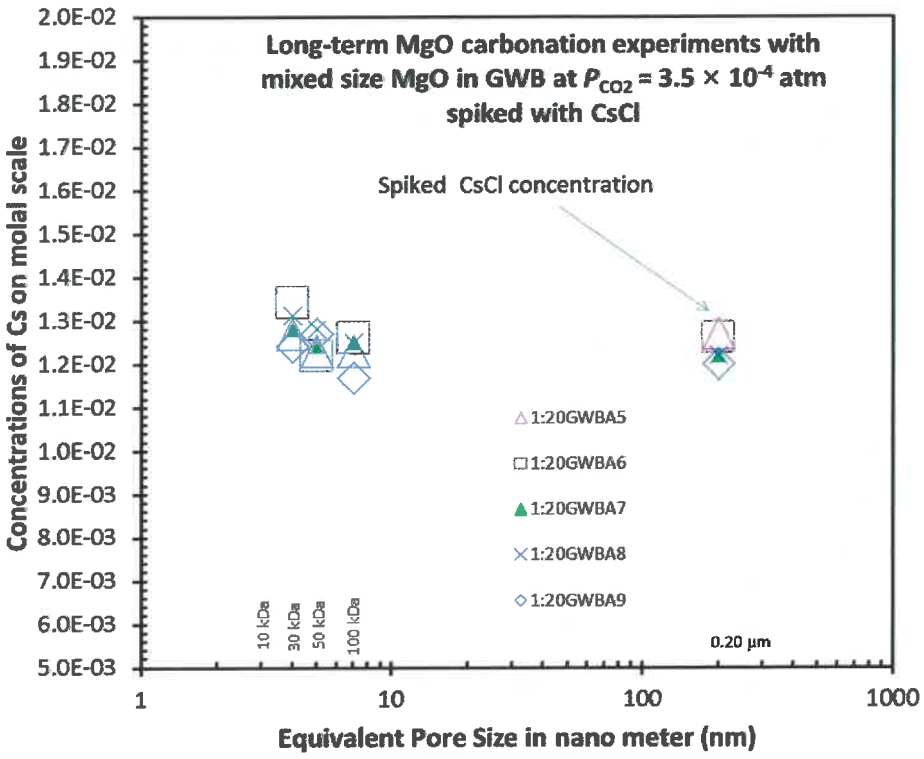

Figure 24

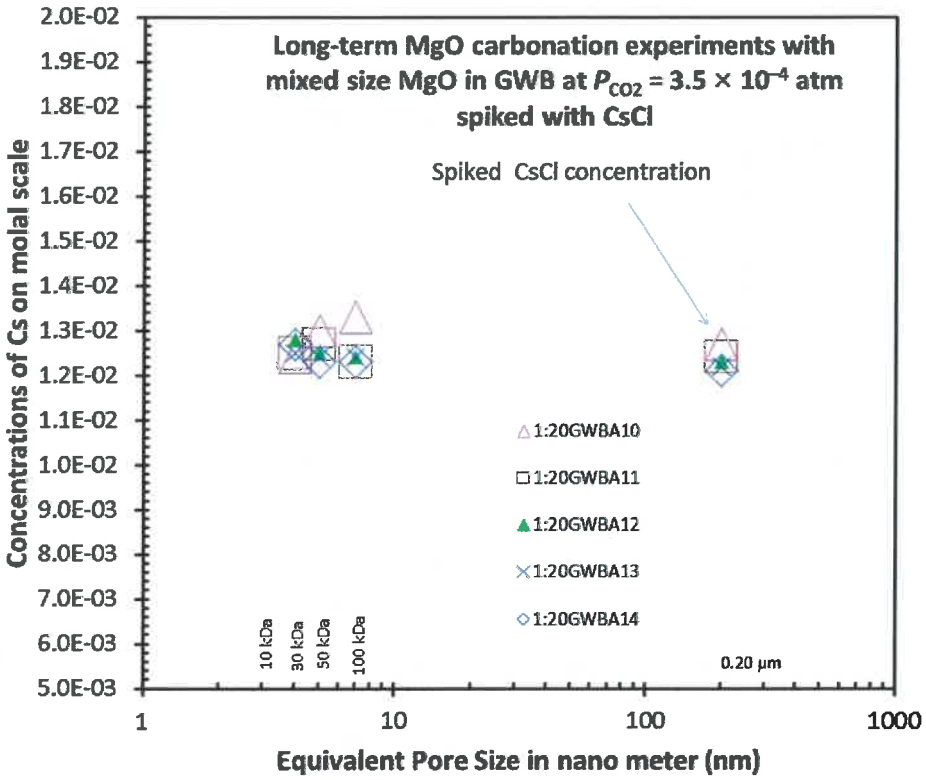

Figure 25

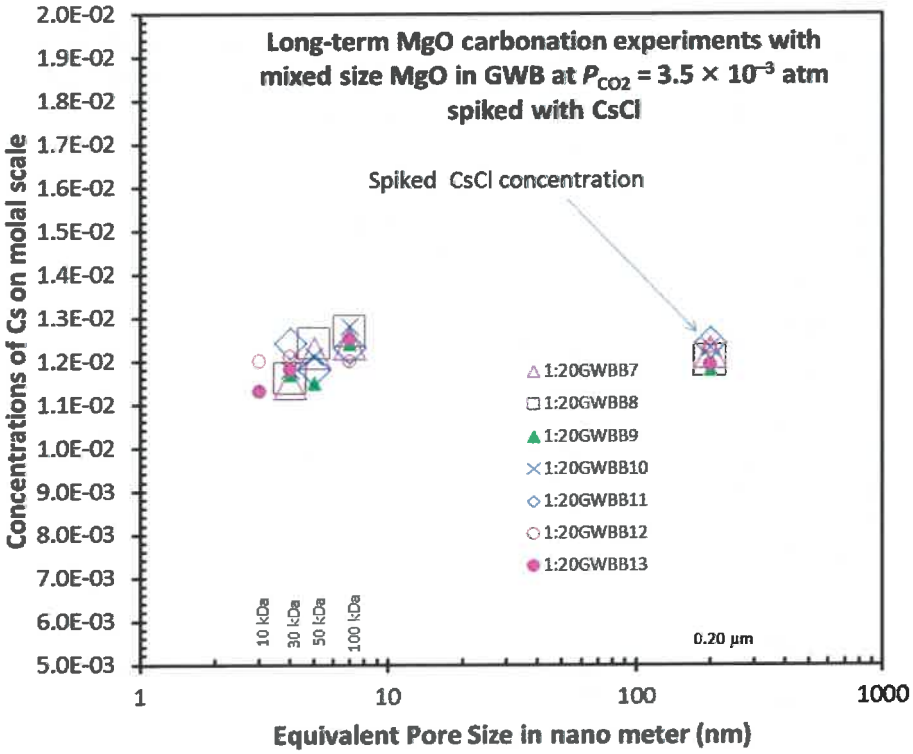

Figure 26

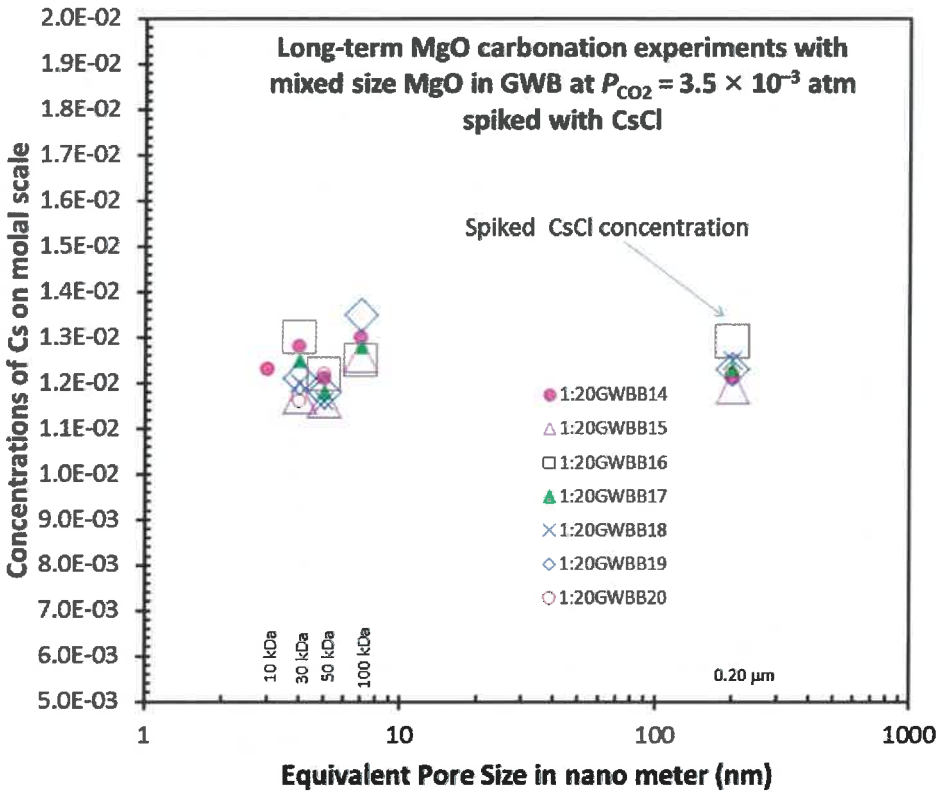

Figure 27

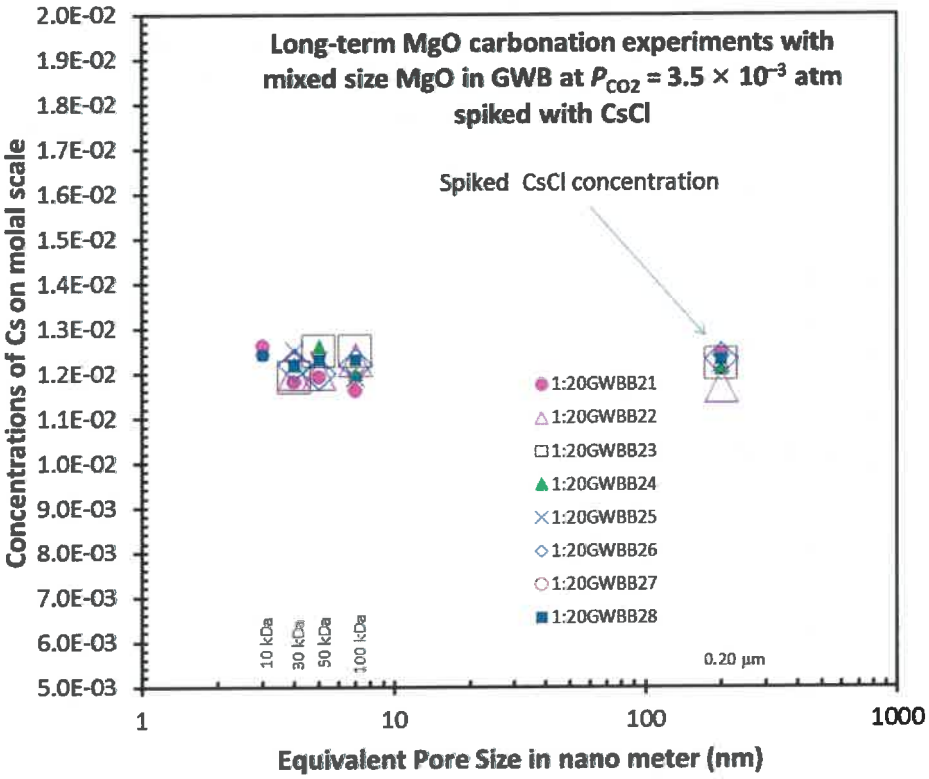

Figure 28

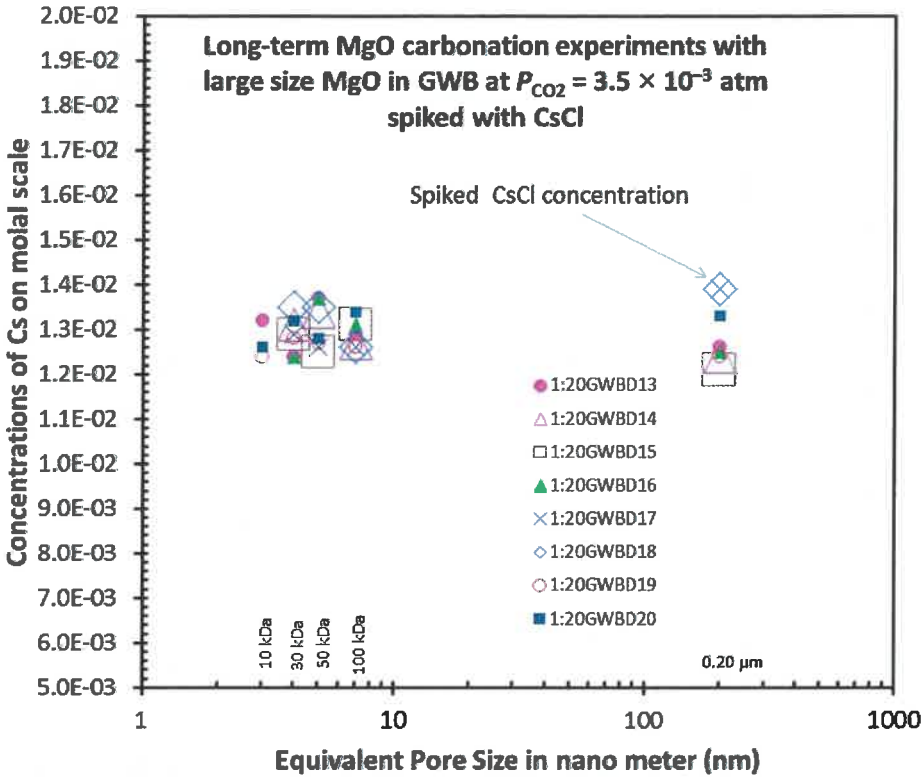

Figure 29

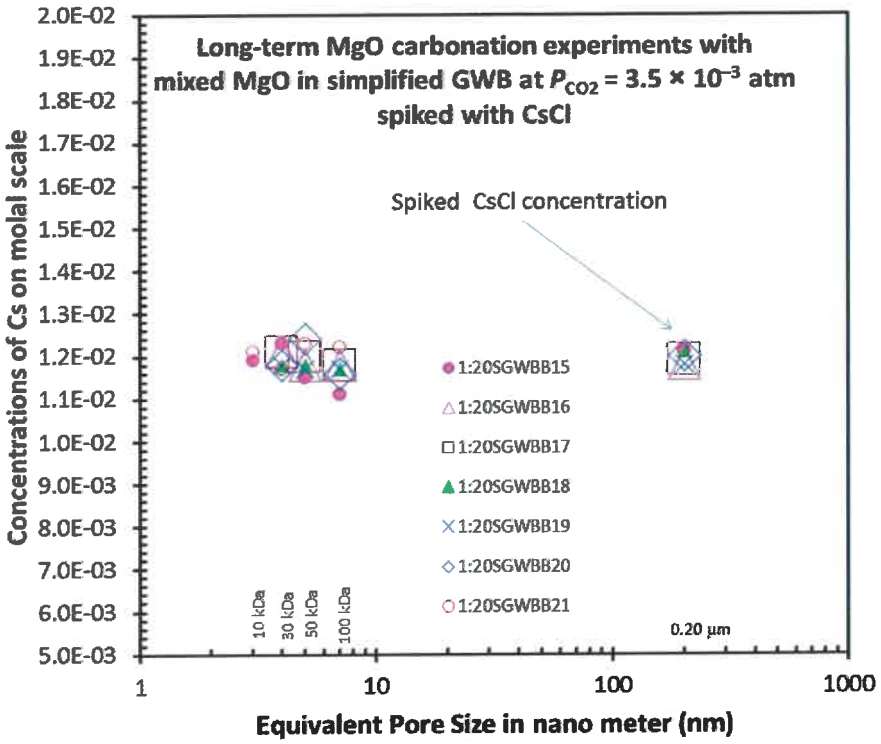

Figure 30

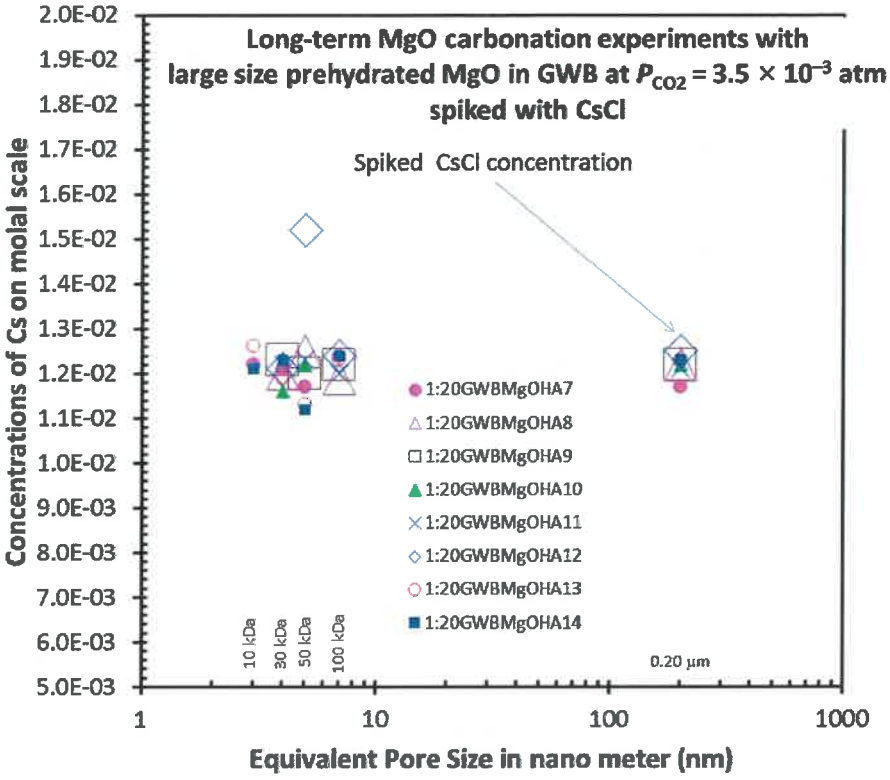

Figure 31

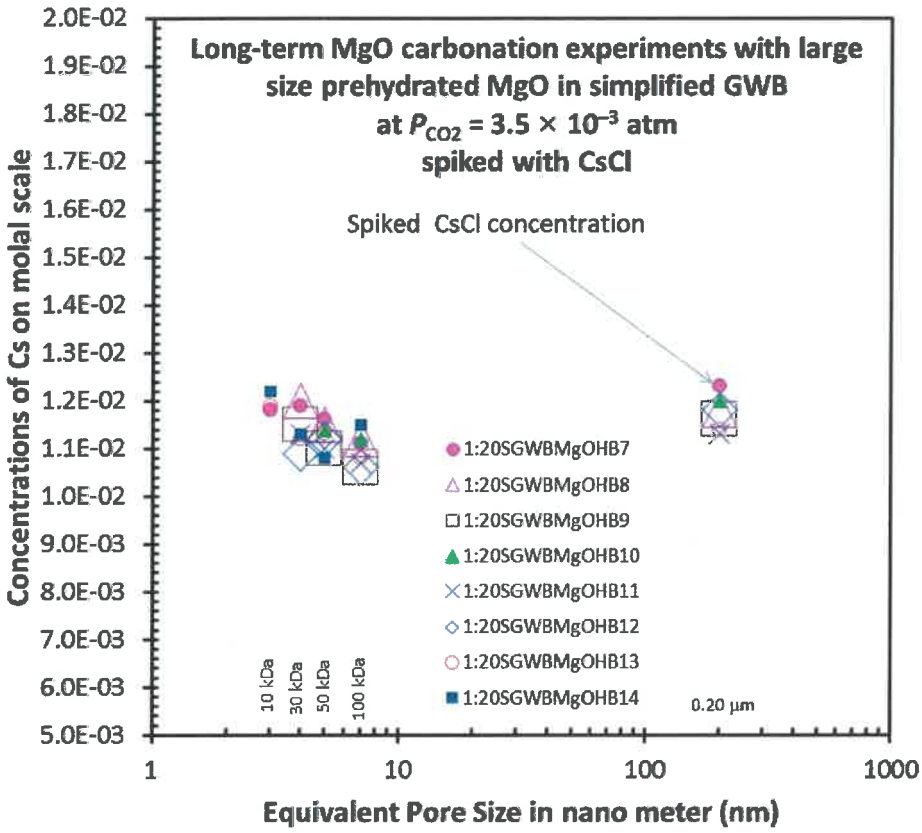

Figure 32